COHERENCE OF UNSTEADY WAKE OF PERIODICALLY PLUNGING AIRFOIL

Burak Turhan, Zhijin Wang, Ismet Gursul

University of Bath, UK

We present an experimental investigation of the flow structure in the near-wake of a NACA0012 airfoil plunging sinusoidally at a chord Reynolds number of Re = 20,000 and for a wide range of reduced frequency k and Strouhal number based on peak-to-peak amplitude St. Estimated mean thrust coefficients using the mean and fluctuating velocity fields confirm St^2 dependence as well as significant effect of the reduced frequency for $k \leq 1$. Generally, time-averaged flow quantities are better correlated with St than k in the range tested ($k \leq 3.14$ and $St \leq 0.24$). Analysis of the streamwise flow and crossflow in the near-wake using two-point cross-correlations and the Proper Orthogonal Decomposition reveal that the unsteady characteristics are even better correlated with St than the mean flow quantities. The percentage energy of the fundamental wake modes of the streamwise flow and the flapping mode of the crossflow increases with increasing St, but at different rates in the drag-producing and thrust-producing wakes. There are similarities with the wake synchronisation behind oscillating bodies. The spanwise length scale is small and in the order of the airfoil thickness for the stationary airfoil. For an oscillating airfoil, the spanwise-averaged cross-correlation coefficient in the measurement domain grows linearly for small St (in the drag-producing wakes), and is nearly constant at a high value for larger St (in the thrust-producing wakes). Results show that the Strouhal number is the most important parameter that determines the degree of two-dimensionality of the wake, and suggest that spanwise vortices are quasi-two-dimensional for $St \geq 0.05$ and $x/c \leq 4$. As the Strouhal number is an amplitude parameter for the wake forcing and determines the degree of two-dimensionality, the implications for experimental gust generators using oscillating airfoils are discussed.

1. Introduction

Unsteady aerodynamics of airfoils and their wakes have received considerable attention due to the relevance to gust loads on aircraft and aeroelasticity of aircraft wings and rotorcraft blades (Theodorsen 1935; Garrick 1936; von Karman and Sears 1938; Sears 1941; McCroskey 1982; Ekaterinaris and Platzer 1998), buffeting, propulsion of swimming animals (Smits 2019), and flapping-wing propulsion of micro air vehicles (Shyy *et al.* 2010). The unsteady forces on an unsteady airfoil are affected by the vorticity shed from the airfoil and the resulting unsteady wake. Early unsteady aerodynamics models were developed in the 1930s based on the attached potential flow assumption (Theodorsen 1935; Garrick 1936; von Karman and Sears 1938; Sears 1941). An important aspect of the assumptions is the two-dimensionality of the vortex sheet shed from the trailing-edge to satisfy the unsteady Kutta condition. However, even if flow separation is fixed at a sharp trailing-edge, it is unlikely that the vorticity shed will remain two-dimensional.

While combined pitching and plunging (heaving) motions have more kinematic parameters, resulting in complex vortex-vortex and vortex-wing interactions, pure plunging motion exhibits all the essential features of oscillating airfoils: vorticity shedding from trailing-edge, roll-up and formation of concentrated vortices, their convection downstream, as well as flow separation at the leading-edge and formation of leading-edge vortices for sufficiently high frequency and amplitude of the motion. Pure plunging motion is a simpler, yet fundamental, model of thrust generation of oscillating airfoils while the geometric angle of attack remains constant.

1.1 Main parameters

There are two main parameters for plunging airfoils: the Strouhal number and reduced frequency. The Strouhal number based on amplitude is:

$$St = f A/U_\infty \tag{1}$$

where $A = 2a$ is the peak-to-peak amplitude of the trailing edge, f is the oscillation frequency, and U_∞ is the free-stream velocity. The Strouhal number is the ratio of the maximum plunge velocity to the freestream velocity. It is also related to the maximum effective angle of attack:

$$\alpha_{eff,max} = tan^{-1}\frac{\pi f A}{U_\infty} = tan^{-1}\pi St \tag{2}$$

if the mean angle of attack is zero. As the maximum effective angle of attack increases with increasing Strouhal number *St* and exceeds a critical value, leading-edge separation and vortex formation may occur. The second parameter, the reduced frequency, is:

$$k = \pi f c/U_\infty \tag{3}$$

where c is the chord length of the airfoil. The reduced frequency k can be considered as the ratio of the time scale of the motion to the convective time scale. Convective motion appears in the wake as the vorticity sheds from the trailing-edge (and also from the leading-edge if there is flow separation) and moves downstream while affecting the flow around the airfoil.

It is widely believed that the Strouhal number *St* is the main parameter that characterizes the unsteady wake for the pure plunging motion (Gursul & Cleaver 2019), although it is also known that two cases with the same *St* but different k do not necessarily produce similar flow fields. Both parameters (*St*, k) appear in the small-amplitude potential flow theory (Garrick 1936). According to Garrick (1936), the time-averaged thrust coefficient varies as St^2, although there is a significant effect of the reduced frequency k (which is often overlooked):

$$C_T = \pi^3 St^2 (F^2 + G^2) \tag{4}$$

where $F(k)$ and $G(k)$ are the real and imaginary parts of the Theodorsen function. The term $(F^2 + G^2) = 1$ at $k = 0$, $(F^2 + G^2) \approx 0.3$ at $k = 1$, and tends to 0.25 for larger k. Therefore, for $k \leq 1$, it is not clear which parameter, if any, may be more dominant in the experiments, not only for the time-averaged quantities, but also for the unsteady characteristics, including the coherence (two-dimensionality) of the oscillating wake.

1.2 Streamwise flow

At low frequencies, a vortex sheet is shed from the trailing-edge with alternating signs (see for example, Cleaver *et al.* 2013). One can view this as a "time-dependent mixing layer" that starts from the oscillating trailing-edge and has a periodically varying velocity differential. A wave-like motion of the wake in the mid-span plane of a high-aspect ratio wing was also reported by Turhan *et al.* (2020). The amplitude of the vortex sheet in the near wake (at $x/c = 5$) increases and can be as high as one order of magnitude larger than the amplitude of the trailing-edge. The coherence of the oscillating wakes at low frequencies has not received much attention so far. At higher frequencies, the vortex sheet rolls into the concentrated vortices, and the cross-

stream distance between the vortices is roughly the same order of magnitude as the peak-to-peak amplitude of the trailing-edge. Intuitively, one may expect improved two-dimensionality and increased coherence of oscillating wakes with increasing frequency. This is based on the observations of the faster roll-up of vorticity into concentrated vortices in the experiments and simulations. On the other hand, the possibility of finding spanwise instabilities also increases once the vortices are fully developed.

Various physical mechanisms may cause three-dimensionality of the oscillating wakes. Separated shear layers, shed from leading-edge or trailing-edge, may exhibit transition. High-fidelity simulations revealed that early signs of the onset of the three-dimensionality of leading-edge vortices can be found at a chord Reynolds number of Re = 10,000 (Visbal 2009). Even an abrupt breakdown of the leading-edge vortex due to the onset of small-scale spanwise instabilities is possible at Re = 40,000. These instabilities may have some similarities to those observed in mixing layers (Bernal and Roshko 1986) and wakes (Williamson 1996). At high frequencies concentrated vortices are fully formed quickly, and as the recent experiments on high aspect ratio wings suggest, spanwise waves with a wavelength of the order of the chord length may appear on the leading-edge vortices (Chiereghin *et al.* 2020; Son *et al.* 2020, 2021a, 2021b; Gao *et al.* 2020).

Another physical mechanism that might affect the coherence of the oscillating wake is related to the natural wake instability, that leads to vortex shedding from the airfoil. This is well known in the bluff body aerodynamics (Bearman 1984). When excited at the natural shedding frequency (and its harmonics or subharmonics), the wake becomes more ordered and synchronized as the vortices lock-in for oscillating cylinders. There are measurements of cross-correlation of the base pressure as a function of spanwise separation distance, but this has not been considered for the flow in the near wake. The data for the wake of oscillating airfoils are not available to the best knowledge of the authors. The only exception is the measurements of cross-correlation in the wake of an oscillating airfoil set at a post-stall angle of attack of 15 deg (Cleaver *et al.* 2011). It was shown that the cross-correlation coefficient for stationary airfoil at Re = 10,000 and for a spanwise separation distance of 1.3c about the mid-span, at x/c = 1, is less than 0.1, but can reach peak values 0.5 to 0.7 when oscillated at the fundamental, subharmonic, and first harmonic of the natural vortex shedding in the wake for A/c = 0.05, resulting in local maxima in the lift coefficient. The vortex lock-in phenomenon in the wake of a plunging airfoil set at zero angle of attack was studied by Young and Lai (2007). In this case,

the natural vortex shedding frequency in the wake was near $k \approx 9.4$ for the NACA0012 airfoil at Re = 20,000. The vortex shedding frequency at this high value of the reduced frequency k at zero angle of attack is beyond the maximum reduced frequency investigated in our experiments ($k \leq \pi$).

As a consequence of the onset of the three-dimensionality of the flow, one may expect a streamwise decay of the vortical structures. Bohl and Koochesfahani (2009) experimentally investigated the downstream development of a pitching airfoil for $x/c \leq 1.1$ at a Reynolds number of Re =12,600, and suggested that the three-dimensionality of the vortices causes faster diffusion of the peak vorticity in the streamwise direction for $k > 5$. Even very small levels of axial velocity along the core of the spanwise vortices can contribute to the decay of the peak vorticity in the streamwise direction. In addition, the turbulent diffusion due to the small-scale motion is likely to reduce the coherence of the vortical flow in the streamwise direction, even if the flow separation at a sharp trailing-edge is two-dimensional.

1.3 Spanwise length scale

In the limiting case of a stationary airfoil set at zero angle of attack, the spanwise correlation length of the near-wake has not received much attention, although there is some prior knowledge for stationary bluff bodies. For nominally two-dimensional wake of a circular cylinder, at a Reynolds number based on the diameter Re_d = 13,000 and in the intermediate wake region x/d = 20, Hayakawa and Hussain (1989) found significant three-dimensionality and estimated the spanwise scale of vortical structures around 1.8d. They concluded that the typical spanwise extent of large spanwise vortices is comparable with the local halfwidth of the wake. Recently, Zhang *et al.* (2021) reported the spanwise length scale to be on the order of 2 to 3 times the thickness H of the body for various D-shaped cylinder wakes, in the range of x/H = 4 - 20 and Re_H = 10,000 to 50,000. Such information for the wakes of stationary and oscillating airfoils is not available to the best knowledge of the authors.

With increasing frequency, although the two-dimensionality of the vortical flow is expected to increase, there is no prior knowledge whether this depends on k or St, and how fast it takes place. There were early attempts to study the three-dimensionality of the flow. Buchner *et al.* (2012) presented some instantaneous 3D flow data in a volume with a spanwise length of 0.12c. David *et al.* (2012) had a spanwise length of 0.35c of the measurement domain. However, the

possibility of finding spanwise waves with larger wavelength (on the order of chord length) exists at high frequencies. It is not clear whether the observations for high aspect ratio wings (Chiereghin *et al.* 2020; Son *et al*. 2020, 2021a, 2021b; Gao *et al.* 2020) are related to those found by the Floquet stability analysis (Sun *et al.* 2018) of the propulsive wake (hence, resulting in a time-averaged jet) of a plunging airfoil set at a zero mean angle of attack at a low Reynolds number of Re = 1,700. It is quite likely that the existence of spanwise instabilities will be dependent on the frequency and the amplitude of the motion. Generally, these instabilities appear at high frequencies, although it is not clear whether the k or St is the determining factor.

Knowledge of the spanwise length scale could be useful not only for the understanding of the unsteady characteristics of oscillating wakes, but also for computational studies. In the *2.5D* simulations of airfoil flows one needs to select a minimal box size in the spanwise direction. Using a Fourier simulation in the spanwise direction requires a periodic length, which needs to be greater than the correlation length, although this choice is also dictated by the desire to capture the largest wavelength of interest. There is currently no experimental data for guidance in choosing the spanwise box size. Visbal (2009) used a spanwise box size of 0.20c in a study of transitional flow over a plunging airfoil at Re = 10,000 to 40,000 at k = 3.93 and A/c = 0.1. Gao *et al.* (2020) and Son *et al.* (2021b) used spanwise box sizes of 2.6c to 5.0c in the Reynolds number range of Re =1,000 to 10,000 in the study of leading-edge vortices and wakes of a plunging airfoil at k = 2 and A/c = 0.5.

1.4 Oscillating wakes as gust generators

Wakes and vortices of oscillating airfoils are often used in wind tunnel experiments as gust generators to simulate downstream wings in gusts. Examples of this type of experimental facilities include the use of oscillating airfoils or cascade of airfoils (Gilman and Bennett 1966; Booth and Yu 1986; Wilder and Telionis 1998; Brion *et al.* 2015; Wei *et al.* 2019a, 2019b, Wu *et al.* 2020), and fixed airfoils with oscillating flaps (Jones and Moore 1972; Bicknell and Parker 1972). The two-dimensionality of the experimentally generated gusts, wakes, and vortices has not been considered so far as a function of generating parameters, such as the frequency and the amplitude of the airfoil motion. Spanwise correlation length must be important when the unsteady forces on the downstream wings are measured and interpreted. While we recognise that specific unsteady characteristics of the unsteady wakes generated by

the above methods will differ, some essential features are expected to be similar. For example, one may expect that the effect of the frequency and the amplitude can be similar. Triantafyllou *et al*. (1991) and Anderson *et al.* (1998) used a generalized Strouhal number based on the total excursion of the trailing-edge of the airfoil for different airfoil motions. Triantafyllou *et al*. (1991) compared the mean thrust coefficient for pure plunging, pure pitching, and combined pitching and plunging motions, and found very good agreement, suggesting that the Strouhal number is the dominant governing parameter. The time-averaged thrust force cannot be interpolated to the wake coherence directly, nevertheless it suggests the importance of the Strouhal number. We believe that the study of the pure plunging motion can shed some understanding of the effects of the reduced frequency k and the Strouhal number St on the wake coherence. It is noted that these parameters determine whether vortices are rolled-up and also a reverse Karman street is generated, and that St is a measure of the amplitude of the wake velocity fluctuations, hence the amplitude of the gust angle.

1.5 Objectives

In this paper we investigate the time-averaged and unsteady characteristics of the wakes of an oscillating airfoil set at zero mean angle of attack at a chord Reynolds number of Re = 20,000 by means of particle image velocimetry (PIV) measurements. The main focus is on the coherence of the oscillating wakes. We investigate the streamwise and spanwise two-point correlations and relative energy of the dominant Proper Orthogonal Decomposition (POD) modes, as well as the time-averaged flow, as a function of the reduced frequency k and the Strouhal number St. The maximum values of the reduced frequency and the Strouhal numbers considered were 3.14 and 0.24, respectively. The paper is organized as follows: Section 2 gives an overview of the experimental set-up, the measurement method and analysis techniques. Discussion of results is presented in Section 3.1 for an overview of the effect of kinematic parameters on the instantaneous flow fields, the mean velocity, and the amplitude of the cross-stream velocity fluctuations as well as an estimate of the drag/thrust coefficient. The two-point cross-correlations and the POD analysis are presented for streamwise flow in Section 3.2 and for crossflow in Section 3.3, and the effects of k and St are discussed. Finally, implications of these findings on the measured unsteady lift force in the wind tunnel gust generators are discussed in Section 3.4.

2. Methods and techniques

2.1 Experimental setup

The experiments were carried out in a closed-loop, free surface water tunnel (Eidetics model 1520) at the University of Bath. The maximum freestream velocity is 0.5 m/s, with a turbulent intensity of around 0.5% (Heathcote 2006). The main test section of the facility is 381 mm wide, 508 mm deep, and 1520 mm long, and tempered glass is used in the test section for the camera and laser access. Figure 1 shows the side and front views of the test section, the test rig, and the schematic of the PIV setup. The airfoil is vertically mounted in the working section. It has a NACA 0012 airfoil profile, an aspect ratio of 5, and a chord length of c = 62.7 mm. The coordinate system is located at the root of the wing at the trailing edge as sketched in Figure 1. The wing was manufactured by selective laser sintering using Polyamide (PA) 2200, with a smooth finish and subsequently spray-painted matte black to eliminate laser reflection during velocity measurements. Nominally two-dimensional airfoil geometry is simulated by using end-plates at both ends, with 2 mm clearance, which extend 2c upstream and 10c downstream of the wing (Chiereghin *et al*. 2019).

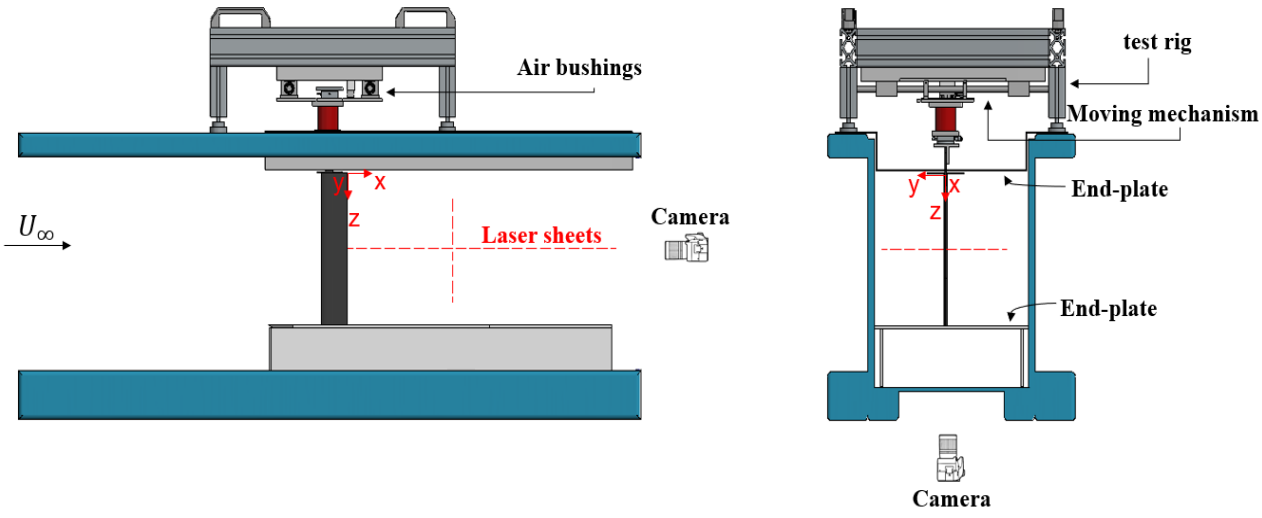

Figure 1 Schematic of the experimental setup and PIV measurements.

The test rig consisted of a fixed platform, which is placed at the top of the water tunnel test section. The wing was connected to the platform through a rotation stage that allowed the wing to rotate, thus adjusting the desired geometric angle of attack with an accuracy of ±0.2º. For this article, the mean angle of attack was set to zero. The plunging motion, provided by a Zaber

LSQ150B-T3 translation stage, was powered by a stepping motor with an X-MCB1 controller. The plunging motion *h(t)* of the airfoil displacement in the cross-stream *y*-direction can be expressed in the form of:

$$h(t) = \frac{A}{2}\cos(2\pi f t) \tag{5}$$

which can be reproduced with an accuracy of 2%. Here the displacement *h(t)* is measured from the mean location of the airfoil ($y = 0$).

2.2 Particle image velocimetry measurements

The particle image velocimetry measurements were conducted at *Re* = 20,000, and geometric angle of attack $\alpha = 0°$. Experiments were carried out at various plunging reduced frequencies (up to $k = 3.14$) and normalized peak-to-peak amplitudes *A/c* (up to 1) as shown in Figure 2. In this amplitude versus frequency plot, maximum values (at fixed amplitude and frequency) are dictated by the limits of the stepping motor, which roughly correspond to a constant value of maximum plunge velocity. The data in Figure 2 result in a maximum value of the Strouhal number *St* = 0.24 in our experiments. As it will be shown, this range of *k* and *St* in our experiments captures the essential features of different flow regimes.

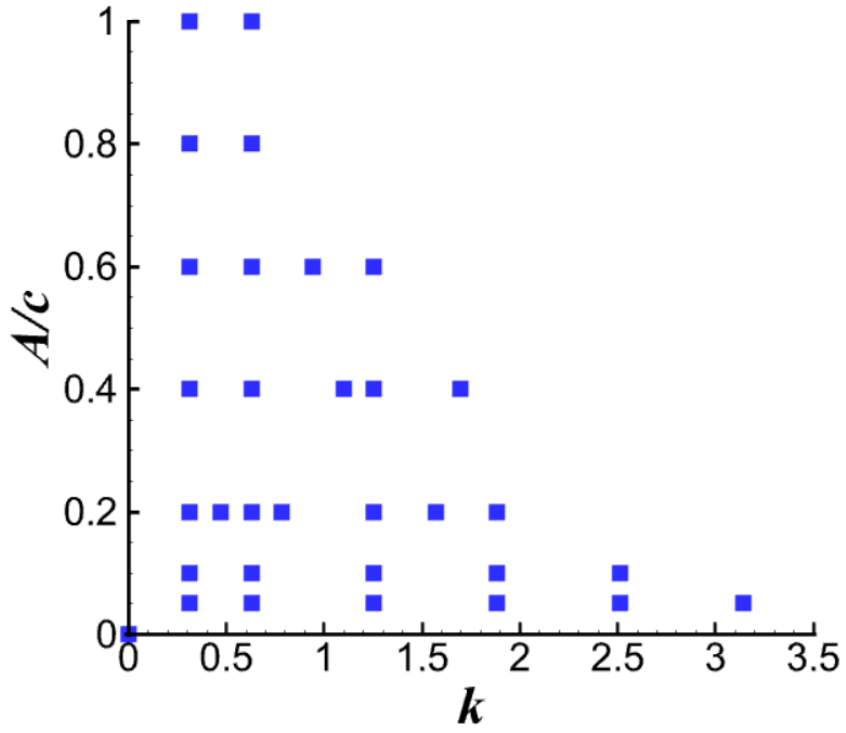

Figure 2 Map of normalized plunge amplitude and reduced frequency values tested.

In this research we performed velocity measurements in two planes: the spanwise plane located at z/c = 2.5 to capture the streamwise flow, and the streamwise plane located at x/c = 4.03 to capture the crossflow. Two laser sheets illuminating the two planes are illustrated in Figure 1. The crossflow PIV measurements were performed in a region which is restricted between z/c = 1 and 4, and has a width of 60% of the span of the airfoil. The measurement region is 1c away from both end-walls in order to avoid the effect of the wall on the vortical flow. For a similar chord length, gap, and Reynolds number, the measurements of Calderon *et al.* (2014) in the same facility suggest that the effect of the wall boundary layer is limited to a region not wider than 0.15c at x/c = 1, which can be taken as a guideline for our measurements at x/c = 4.03.

The PIV system is a commercially available TSI system that consists of a synchroniser (TSI model 610036), a double-pulsed laser (Nd: YAG 50mJ), and an 8 MP camera. The data sampling rate was chosen as 3.75 Hz (which was not a subharmonic or higher harmonic of the plunging frequency) for continuous sampling of sequential 2,000 instantaneous flow fields. The time interval between two laser pulses was Δt = 0.8 ms. The water was seeded with commercially available hollow glass spheres (8-12 μm in diameter). The images were processed via algorithms provided by TSI's software package INSIGHT 4GTM using Fast Fourier Transform (FFT). The image processing was carried out with an interrogation window size of 32 by 32 pixels with 25% overlap, resulting in a spatial resolution of 2.5%c. The time-averaged data are derived from the 2,000 pairs of images for each case. The primary peak ratio (PPR) algorithm for PIV uncertainty has been implemented and calibrated within INSIGHT 4GTM for each set of PIV processing parameters. The instantaneous measurement uncertainty was obtained using the PPR method with expanded uncertainty within a 95% confidence level (Charonko and Vlachos 2013). The mean value of uncertainty was around 2% of the free stream velocity. We also estimated the uncertainty of momentum thickness as 3% and thrust coefficient as 8%.

2.3 Proper orthogonal decomposition

The proper orthogonal decomposition (POD) method has been extensively used for unsteady flows. The method extracts the significant properties that may otherwise be hidden within flow structures and instantaneous snapshots. In experimental studies, this method helps to interpret PIV data and reveal the most energetic modes. The POD is used to decompose the coherent

large-scale flow unsteadiness as a spatial vector function and extract the spatially most energetic eigenfunctions of the flow. The corresponding eigenvector represents the basis function or mode shape (Sirovich 1987; Berkooz *et al.* 1993). For example, the POD method decomposes the cross-stream velocity component as shown below:

$$v(x,y,t) = V(x,y) + v'(x,y,t) = V(x,y) + b_1(t)POD_1(x,y) + b_2(t)POD_2(x,y) + \cdots \quad (6)$$

where V is the mean cross-stream velocity component, and v' is the fluctuating cross-stream velocity component of the velocity field. Here *POD* and *b* are modes and corresponding mode coefficients. For oscillating wakes of plunging airfoils, most of the energy in the flow can be captured in the first few modes. In this paper, the analysis was performed using commercial software TSI GRAD-POD TOOLBOX, which employs the spatial-temporal data analysis technique proposed by Heiland (1992).

2.4 Two-point cross-correlations

The two-point correlations are used to determine the length scales associated with the coherent flows. The two-point correlation is defined (Bendat and Piersol 1986) below for the cross-stream velocity component:

$$C_{vv} = \frac{\sum_{i=1}^{n}(v_A(t) - V_A)(v_B(t) - V_B)}{\sqrt{\sum_{i=1}^{n}(v_A(t) - V_A)^2}\ \sqrt{\sum_{i=1}^{n}(v_B(t) - V_B)^2}} \quad (7)$$

where v_A is the cross-stream velocity component at the reference point *A*, and v_B is the cross-stream velocity component at the spatial location *B* in the measured velocity field. In this paper, we calculated the two-point correlations of the cross-stream component in the *x*-*y* plane at the midspan of the airfoil (*z*/*c* = 2.5) and in the *y*-*z* (crossflow) plane at *x*/*c* = 4.03. In the *x*-*y* plane the reference point was taken as (*x*/*c* = 0.5, *y*/*c* = 0) and in the *y*-*z* plane the reference point was taken as (*z*/*c* = 2.5, *y*/*c* = 0).

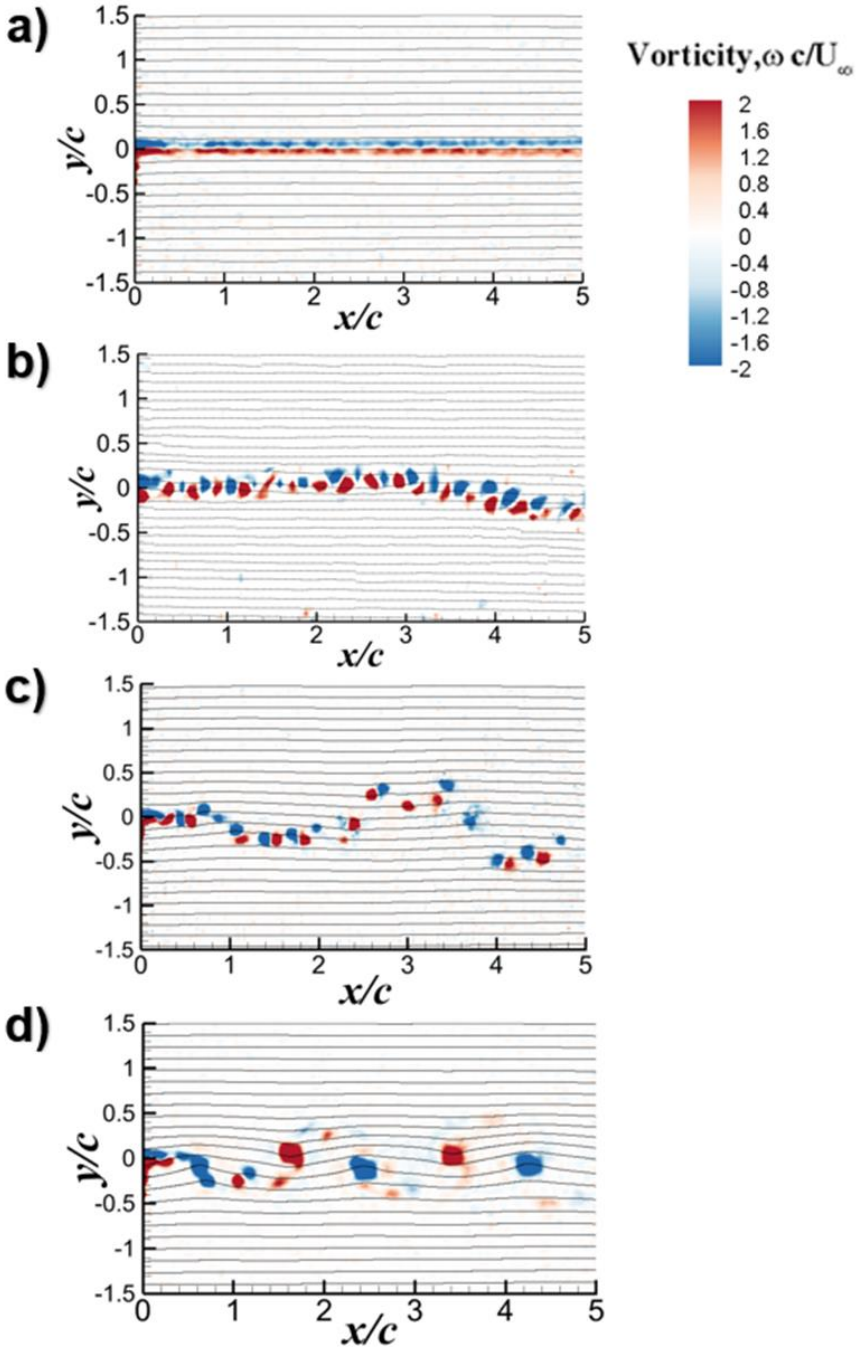

Figure 3 Instantaneous vorticity contours at a fixed value of A/c = 0.1 for a) k = 0, b) k = 0.63, St = 0.02, c) k = 1.26, St = 0.04, and d) k = 1.88, St = 0.06.

3. Results

3.1 Overview of streamwise flow

We start with the effects of the oscillation frequency and amplitude of the plunging motion on the main features of the instantaneous flow, followed by the summary of the effects of the main

dimensionless parameter k and St on the time-averaged quantities, including the mean streamwise velocity and the amplitude of the cross-stream velocity fluctuations.

Figure 3 presents the instantaneous vorticity together with streamlines in the wake for A/c = 0.1 and varying frequency, including the case of the stationary airfoil (k = 0). For the stationary airfoil, the vorticity sheets of opposite sign shed from the airfoil roll up into small concentrated vortices in the wake. The wavelength of the vorticity concentrations can be estimated from this instantaneous image as approximately 0.3c. A more accurate time-averaged estimate can be obtained by means of two-point correlation measurements as will be presented in the next section. The approximate wavelength of 0.3c for the wake of the stationary wake can also be used to obtain an estimate of the frequency of the wake vortex shedding (the present PIV measurements are not time-resolved). If the convection velocity is assumed to be equal to the freestream velocity in the wake, one finds the reduced frequency of vortex shedding as $k \approx 10$, which is comparable to the prediction of the two-dimensional unsteady laminar flow simulations of Young and Lai (2007) as $k \approx 9.4$ for the same airfoil and Reynolds number. As will be discussed later, the spanwise length scale for this case drops to around $L \approx 0.16c$ at x/c = 4.03. Considering the lack of two-dimensionality in the experiments, the success of two-dimensional simulations is remarkable. As the plunge oscillation frequency is increased in Figure 3, small vorticity concentrations are still visible while the large-scale travelling wave motion of the wake reaches a peak-to-peak amplitude that is one order of magnitude larger than that of the airfoil motion (A/c = 0.1) at k = 1.26 (St = 0.04). With further increase in the reduced frequency to k = 1.88 (St = 0.06), a reverse Karman vortex street is observed, which is generally associated with thrust generating wakes. (It is known that the change in the vortex configuration does not exactly coincide with the change from drag to thrust (Bohl and Koochesfahani 2009)).

Figure 4 shows the instantaneous vorticity together with streamlines in the wake for a fixed reduced frequency k = 1.26 and varying amplitude A/c (hence the Strouhal number based on amplitude St as well). With increasing amplitude A/c, one can see the increasing amplitude of the large-scale travelling wave motion of the wake, but not as fast as it increases with frequency. Therefore, there is a suggestion of k being a more important parameter as far as the amplitude of the wake shear layer is concerned. This is also reinforced by the comparison of the two cases with the same Strouhal number St: (k = 0.63, St = 0.02) in Figure 3 and (k = 1.26,

St = 0.02) in Figure 4. For the largest amplitude shown in Figure 4, once again there is thrust producing wake with a relatively large vertical distance between the two rows.

The variations of the normalized mean stream velocity defect or excess and the normalized root-mean-square (rms) of the cross-stream velocity fluctuations at *x/c* = 4.03 are shown in

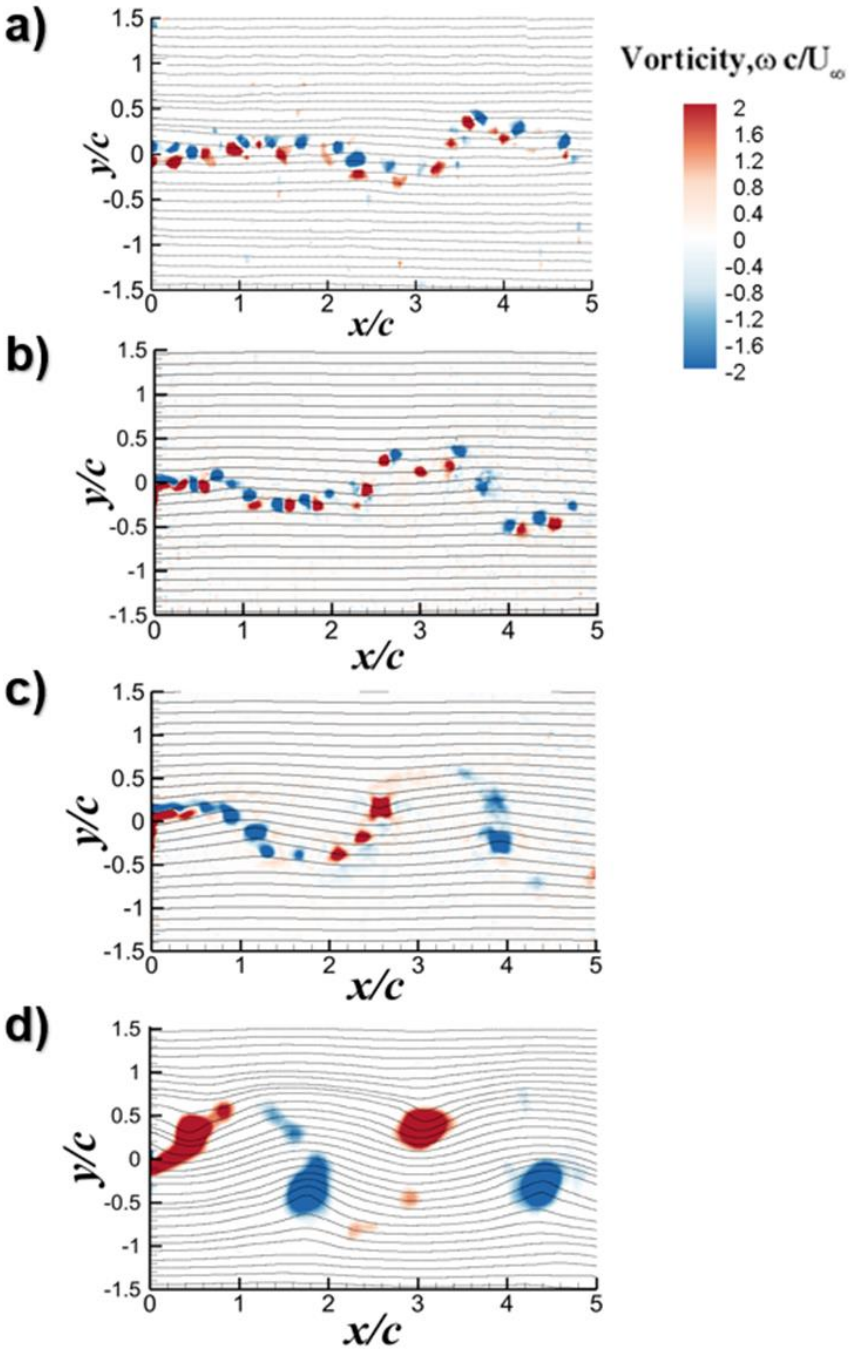

Figure 4 Instantaneous vorticity contours at a fixed value of *k* = 1.26 for a) *A/c* = 0.05, *St* = 0.02, b) *A/c* = 0.1, *St* = 0.04, c) *A/c* = 0.2, *St* = 0.08, and d) *A/c* = 0.4, *St* = 0.16.

Figure 5(a) and 5(b), which correspond to the cases shown in Figure 4 together with the stationary airfoil case. The wake-like mean velocity profile seen for the stationary airfoil becomes jet-like only for $St \geq 0.08$, whereas the mean velocity profile is not simply jet-like or wake-like for lower values of the Strouhal number. The corresponding variation of the rms of the cross-stream velocity profiles in Figure 5(b) reveal that the single peak of the stationary

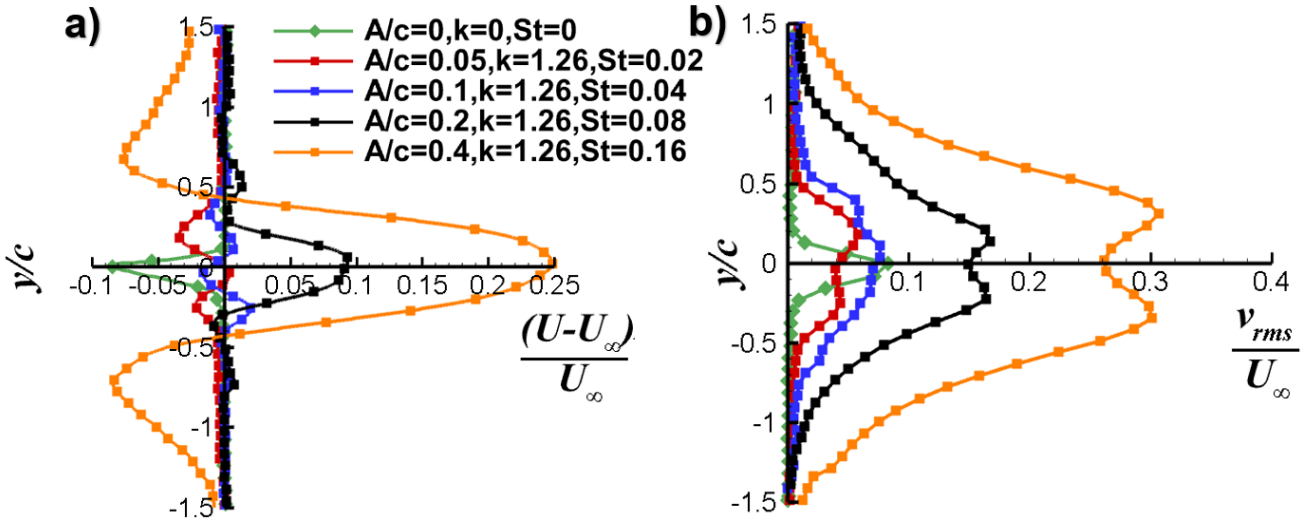

Figure 5 Variation of a) time-averaged streamwise velocity deficit/excess, b) rms of cross-stream velocity fluctuations of the stationary and oscillating airfoil for the same reduced frequency (k = 1.26) and various amplitudes; x/c = 4.03.

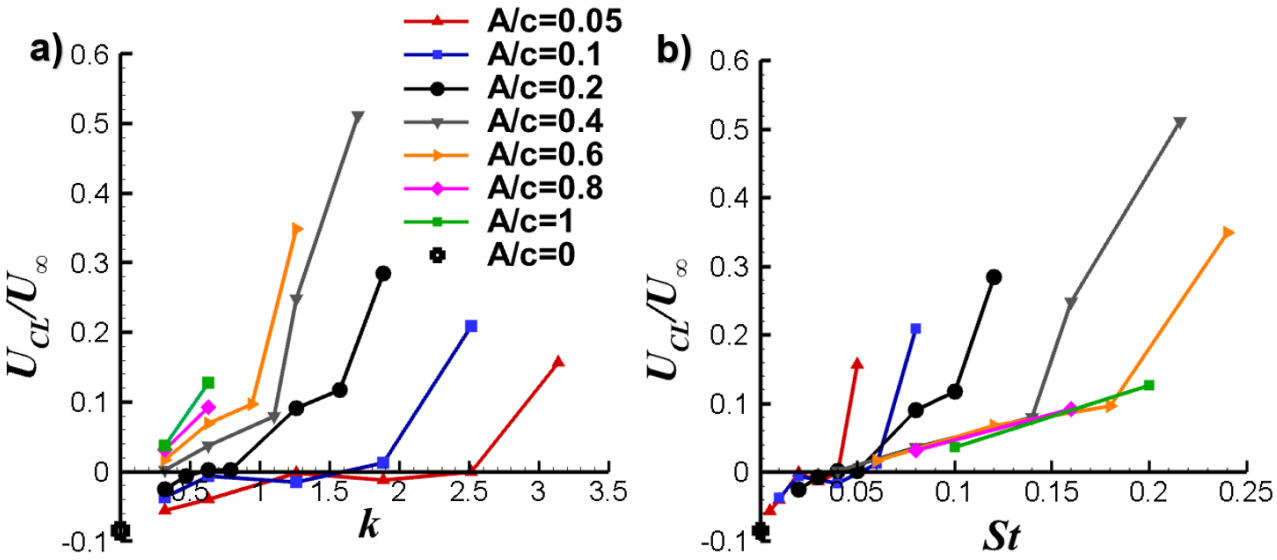

Figure 6 The mean streamwise velocity at the centreline (x/c=4.03 and y/c=0) for all cases as a function of a) reduced frequency, b) Strouhal number.

airfoil develops into double-peaks located at approximate cross-stream coordinates of the row of the vortices in Figure 4 for the largest plunge amplitude.

The normalized mean streamwise velocity at the wake centerline at x/c = 4.03 is shown for all cases as a function of the reduced frequency k in Figure 6(a) and the Strouhal number St in Figure 6(b). Whereas the reduced frequency k does not reveal any collapse of the data, the mean centerline velocity generally increases with increasing k and A/c. In contrast, there is a trend of the data to collapse with St, except for higher frequencies at each fixed amplitude A/c. The corresponding variation of the normalized rms velocity of the cross-stream velocity component is shown as a function of the reduced frequency k in Figure 7(a) and the Strouhal number St in Figure 7(b). It increases almost linearly with increasing k for lower values of k. When compared with the mean velocity at centerline in Figure 6, the maximum rms velocity fluctuations exhibit similar trends with k and St. Again, a slightly better collapse with St for lower values of k is evident in Figure 7(b). Clearly no single parameter is sufficient to provide a good collapse in Figures 6(b) and 7(b) as both St and k are the main parameters. However, there is clearly better correlation with St. This is expected because the Strouhal number is an amplitude parameter (the ratio of the maximum plunge velocity to the freestream velocity).

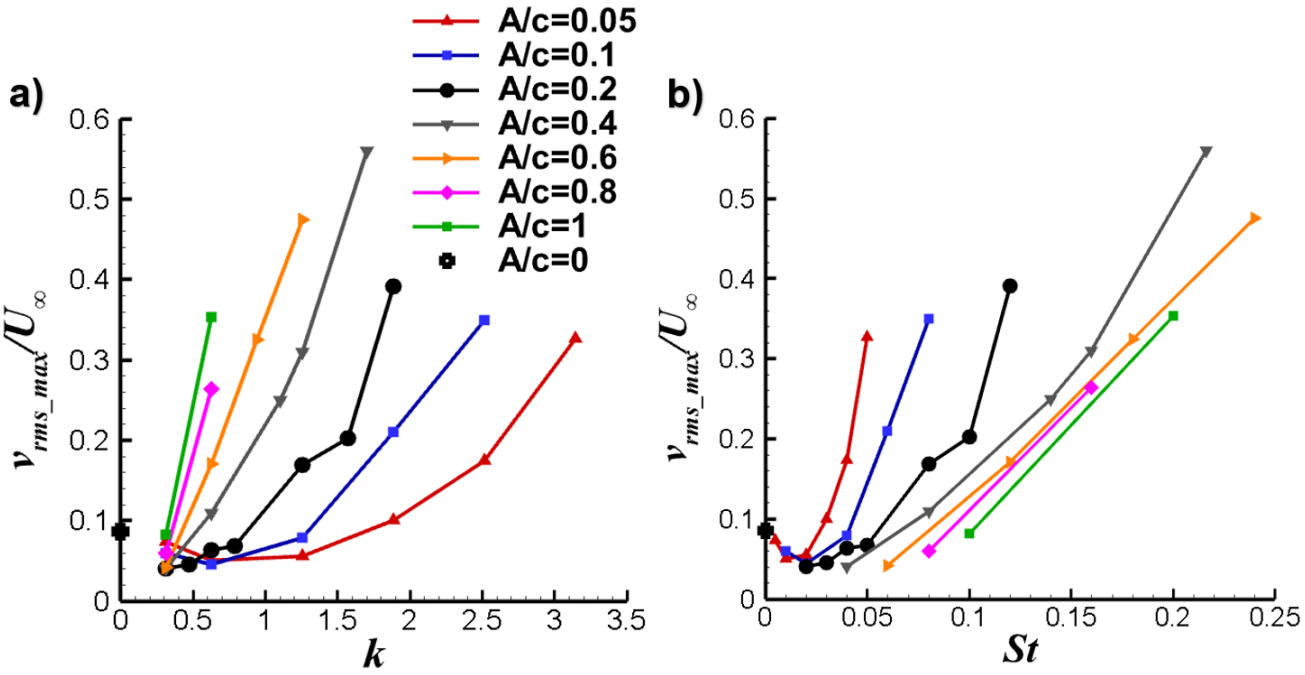

Figure 7 The maximum rms cross-stream velocity fluctuation (v_{rms}) at x/c = 4.03 for all cases as a function of a) reduced frequency, b) Strouhal number.

The variation of the momentum thickness,

$$\theta = \int_{-\infty}^{\infty} \frac{U}{U_\infty}\left(\frac{U}{U_\infty} - 1\right) dy \tag{8}$$

normalized by the chord length at x/c = 4.03 is shown as a function of the reduced frequency k in Figure 8(a) and the Strouhal number St in Figure 8(b). Interestingly, the collapse of the data with St is very good for the whole range of the data. It is interesting that an integral quantity exhibits a clear collapse with respect to St, while the localised quantities in Figures 6 and 7 do not collapse as clearly. A rough approximation for the thrust coefficient can be obtained as:

$$C_T = \frac{2\theta}{c} \tag{9}$$

(see Squire and Young 1937, for example). It was shown that estimated thrust coefficients based on the mean velocity can be erroneous in highly unsteady wakes of oscillating airfoils (Bohl and Koochesfahani 2009). It was found that the rms of the velocity fluctuations in the streamwise direction u_{rms} and in the cross-stream direction v_{rms} can make significant contribution to the time-averaged momentum coefficient. Bohl and Koochesfahani (2009) also took into account the downstream mean velocity at the border of the control volume, which may be slightly different from the freestream velocity. The corrected thrust coefficient using the full formulation of Bohl and Koochesfahani (2009) is compared with the direct measurements of the thrust force with force balances (Heathcote *et al.* 2008; Cleaver *et al.* 2013) in Figure 9(a).

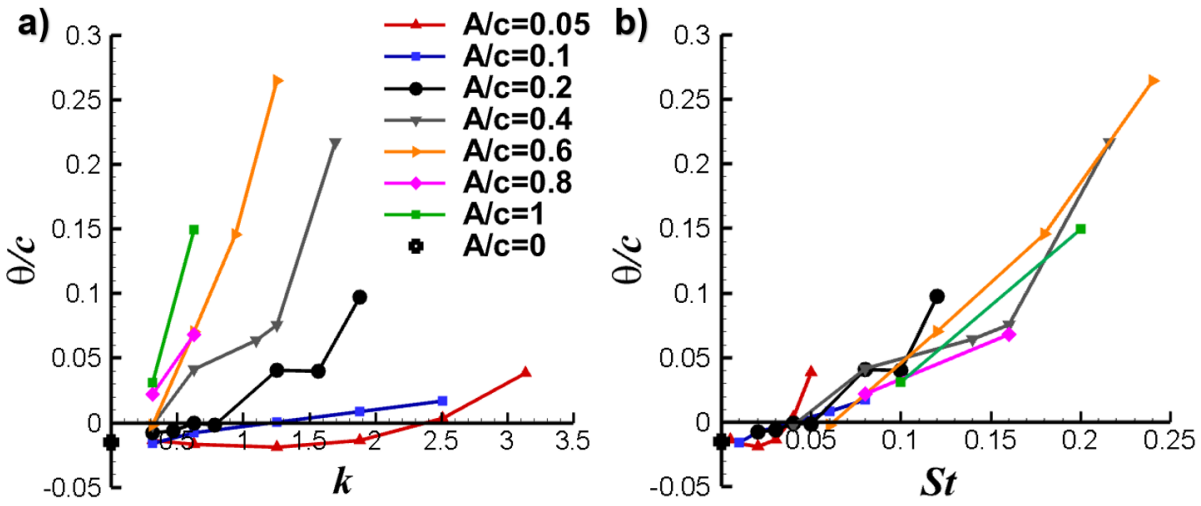

Figure 8 Variation of momentum thickness for all cases as a function of a) reduced frequency, b) Strouhal number.

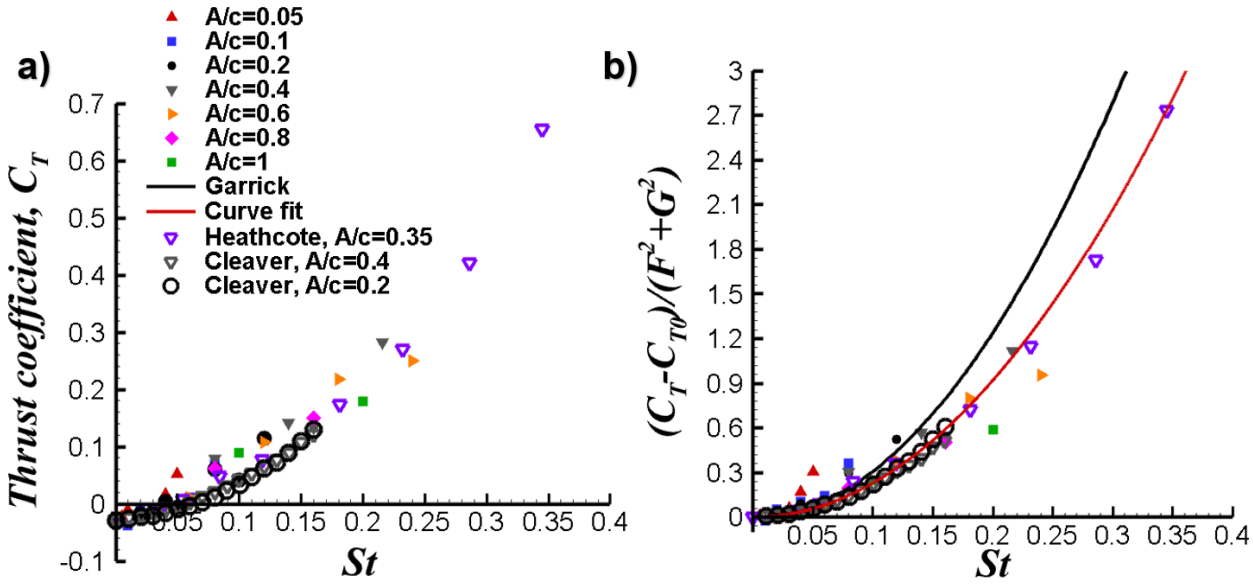

Figure 9 Variation of a) estimated thrust coefficient and comparison with the results of direct force measurements from the literature; b) $(C_T - C_{T0})/(F^2 + G^2)$ as a function of Strouhal number.

For the stationary NACA 0012 airfoil at this Reynolds number, close agreement was found between the estimated thrust (drag) coefficient (C_{T0} = –0.027) and the values reported by Heathcote *et al.* (2008) (C_{T0} = –0.028) and Cleaver *et al.* (2013) (C_{T0} = –0.029) using direct force measurements, and Koochesfahani (1989) (C_{T0} = –0.027) using the momentum equation. At this Reynolds number, drag force switches to thrust force at approximately $St \approx 0.05$. Although the agreement between the estimated and directly measured thrust is reasonably good, there are still deviations for some data points, which are usually those with larger k values at each amplitude A/c. This raises the possibility of increasing influence of k with increasing reduced frequency. As discussed in the Introduction (Section 1.1), Garrick's theoretical prediction already points out a decrease of more than 70% at high reduced frequencies ($k \geq 1$) compared to the value at $k = 0$. In order to separate the effects of reduced frequency and also to be able to make a comparison with the Garrick's inviscid theory (1936), his prediction of the thrust coefficient (see Section 1.1) is written here as:

$$\frac{C_T - C_{T0}}{F(k)^2 + G(k)^2} = \pi^3 St^2 \qquad (10)$$

The quantity on the left-hand side was calculated based on the estimated thrust coefficient from our experiments and plotted in Figure 9(b). For each experimental data point, there are corresponding values of *k* and *St* based on kinematic parameters such as frequency and plunge amplitude. In Figure 9b, for each data point, the corresponding values of the functions *F(k)* and *G(k)* were calculated while the thrust coefficient term $(C_T - C_{T0})$ was estimated based on the full formulation of Bohl and Koochesfahani (2009) to yield $(C_T - C_{T0})/(F^2 + G^2)$. The solid black curve corresponds to the Garrick theory. It is seen that the experimental data still have scatter as much as Figure 9(a). It is also noted that, although the agreement with the Garrick theory is not as good, a parabolic curve fit, shown with a red solid line,

$$\frac{C_T - C_{T0}}{F(k)^2 + G(k)^2} = 23\,St^2 \tag{11}$$

provides a better approximation to our data and the others. The coefficient of the parabolic curve fit is approximately 74% of π^3 of the Garrick theory.

The change of the constant in front of the parabola St^2 in the above equation may also be interpreted as a change of the reduced frequency effect of $\pi^3(F^2 + G^2)$ to $23(F^2 + G^2)$. The reduced frequency dependence remains with the same function shape, but multiplied by a different constant. As the Garrick prediction assumes that the wake remains planar, the experimentally found coefficient can be considered as a correction for the roll-up of vortex sheets.

3.2 Coherence of streamwise flow

The two-point cross-correlations and the POD modes presented in this section capture the wave-like motion in the wake and the wavelength, and also reveal the decay of the amplitude of the cross-correlations. In addition, the POD modes show the dominant structures and confirm that *St* is the main parameter.

Figure 10 shows the contours of the cross-correlation coefficient of the cross-stream velocity fluctuations measured at two points. The reference point is taken at (*x/c* = 0.50, *y/c* = 0) for all cases presented here. The cross-correlation of the cross-stream velocity fluctuations between the reference point and any arbitrary point for all cases are shown in the left column. In the right column, the variation of the cross-correlation coefficient C_{vv} (*x/c*, *y/c* = 0) is shown for

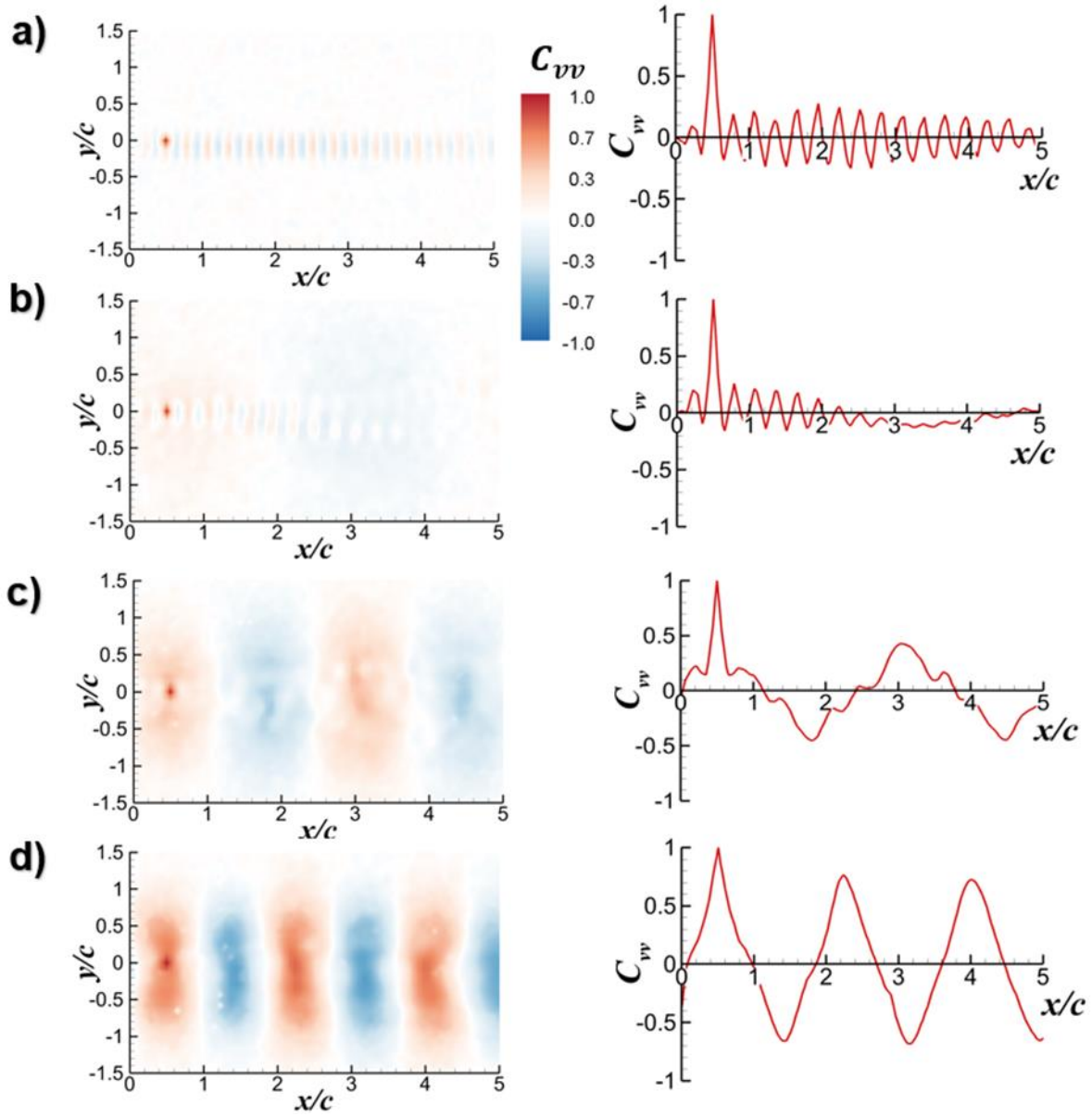

Figure 10 Contours of cross-correlation of cross-stream velocity component C_{vv} (left column); its variation in the streamwise distance at y/c=0 (right column) for A/c = 0.1 and a) stationary airfoil, b) k = 0.63, St = 0.02, c) k = 1.26, St = 0.04, and d) k = 1.88, St = 0.06.

clarity. The cases shown in this figure correspond to the instantaneous vorticity fields shown in Figure 3. For the stationary airfoil, the wake instability and the vortex shedding from the airfoil can be clearly identified. An average wavelength of 0.29c was found in this case. For the smallest plunge frequency (k = 0.63, St = 0.02) shown in Figure 10(b), the natural vortex shedding instability can still be observed in the near-wake, but decaying further downstream. With further increase in the frequency shown in Figure 10(c) and 10(d), the peak cross-correlation coefficient increases, while the wavelength of the vortical motion can be easily

calculated from the cross-correlation coefficient contours. For $k > 0.70$, the mean convection velocity is within $U_c/U_\infty = 1.0$ to 1.1, increasing with increasing St (not shown here).

Figure 11(a)-(d) presents the first two dominant POD modes of the cross-stream velocity component for the corresponding cases. In each case the first two modes have approximately the same percentage of the total energy, and contain much larger energy than the rest of the modes, as shown in Figure 11(e). These two modes characterize the travelling wave in the wake, corresponding to the fundamental frequency, and therefore we call them fundamental "wake modes". The second mode is shifted quarter-wavelength with respect to the first mode. For the two largest reduced frequency cases shown in Figure 11, the main wake modes appear roughly circular with decreasing wavelength. It is also seen in Figure 11(e) that the relative energy of the first two modes increases with increasing frequency (reduced frequency k and Strouhal number St) at the fixed value of $A/c = 0.1$.

Figures 12 and 13 show the contours of cross-correlation coefficients and the POD modes of the cross-stream velocity fluctuations for the cases shown in Figure 4. The effects of increasing amplitude A/c (and, also St) at a fixed reduced frequency k, can be seen in these figures. For the smallest amplitude $A/c = 0.05$ in Figure 12, the natural wake shedding instability just downstream of the oscillating airfoil still exists, decaying further downstream. With increasing amplitude, the peak cross-correlation coefficient (downstream of the reference point) increases, while the wavelength remains roughly constant. The wave-like motion, including the amplitude decay, is captured in these plots. The cross-stream extent of the cross-correlation coefficient also increases with increasing amplitude.

In Figures 10 and 12, for Strouhal numbers up to and including the case of $St = 0.04$, the natural vortex shedding can be detected. For $St = 0.06$ and higher, there is no sign of natural vortex shedding. Karniadakis & Triantafyllous (1989) studied the response of laminar wakes behind circular cylinders at $Re = 100$ as periodic excitation is applied. Lock-in and non-lock-in of vortices, resulting in periodic, quasi-periodic, or chaotic flow response were observed depending on the combination of the amplitude and frequency of the forcing. The response can be qualitatively represented by a "resonant horn" or "Arnol'd" diagram. Young & Lai (2007) presented a similar diagram for the wake of a NACA0012 airfoil in plunging motion at a Reynolds number $Re = 20{,}000$ using two-dimensional simulations. In both studies cited above, the key parameters are the ratio of the excitation (forcing) frequency to the natural vortex

shedding frequency and the amplitude of the forcing (plunge amplitude in the case of Young & Lai (2007)). In our experiments, the natural vortex shedding frequency has a reduced frequency of $k \approx 10$, hence the frequency ratio is less than 0.31 for all cases. For low frequency ratios, Young and Lai (2007) provide an approximate boundary for vortex lock-in, which we calculated as corresponding to St = 0.03 to 0.06. Given the 2D nature of their simulations, it is remarkable that we also find a region of low coherence (both in streamwise and spanwise directions) for St less than 0.05.

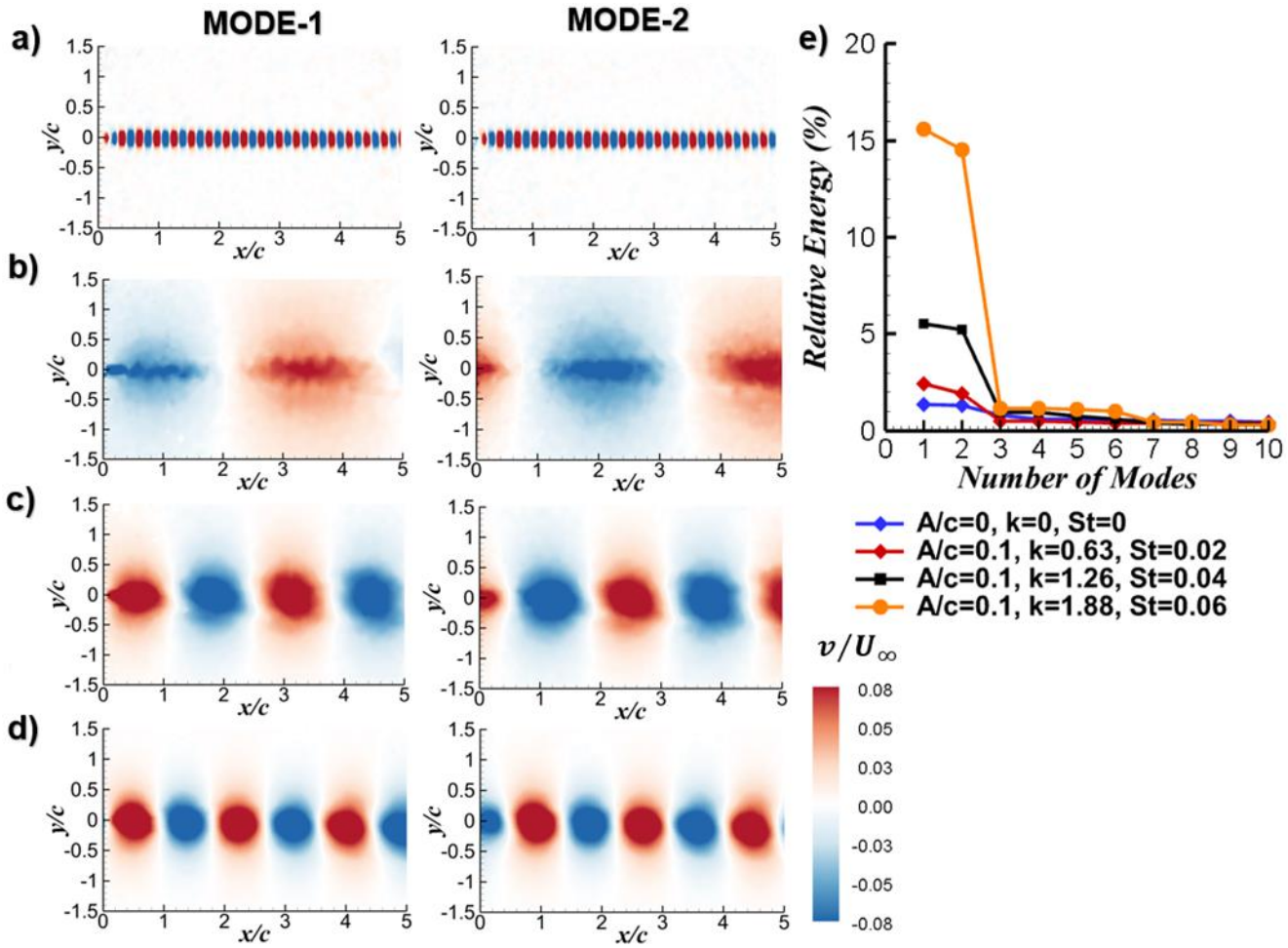

Figure 11 First two POD modes of cross-stream velocity component for A/c = 0.1 and a) stationary airfoil, b) k = 0.63, St = 0.02, c) k = 1.26, St = 0.04, d) k = 1.88, St = 0.06; e) ratio of the energy of mode to the total energy.

Figure 13(a)-(d) presents the first two dominant POD modes of the cross-stream velocity component for the corresponding cases. Again, the first two modes, characterizing the travelling main wake modes, are the most energetic modes compared to all other modes, and

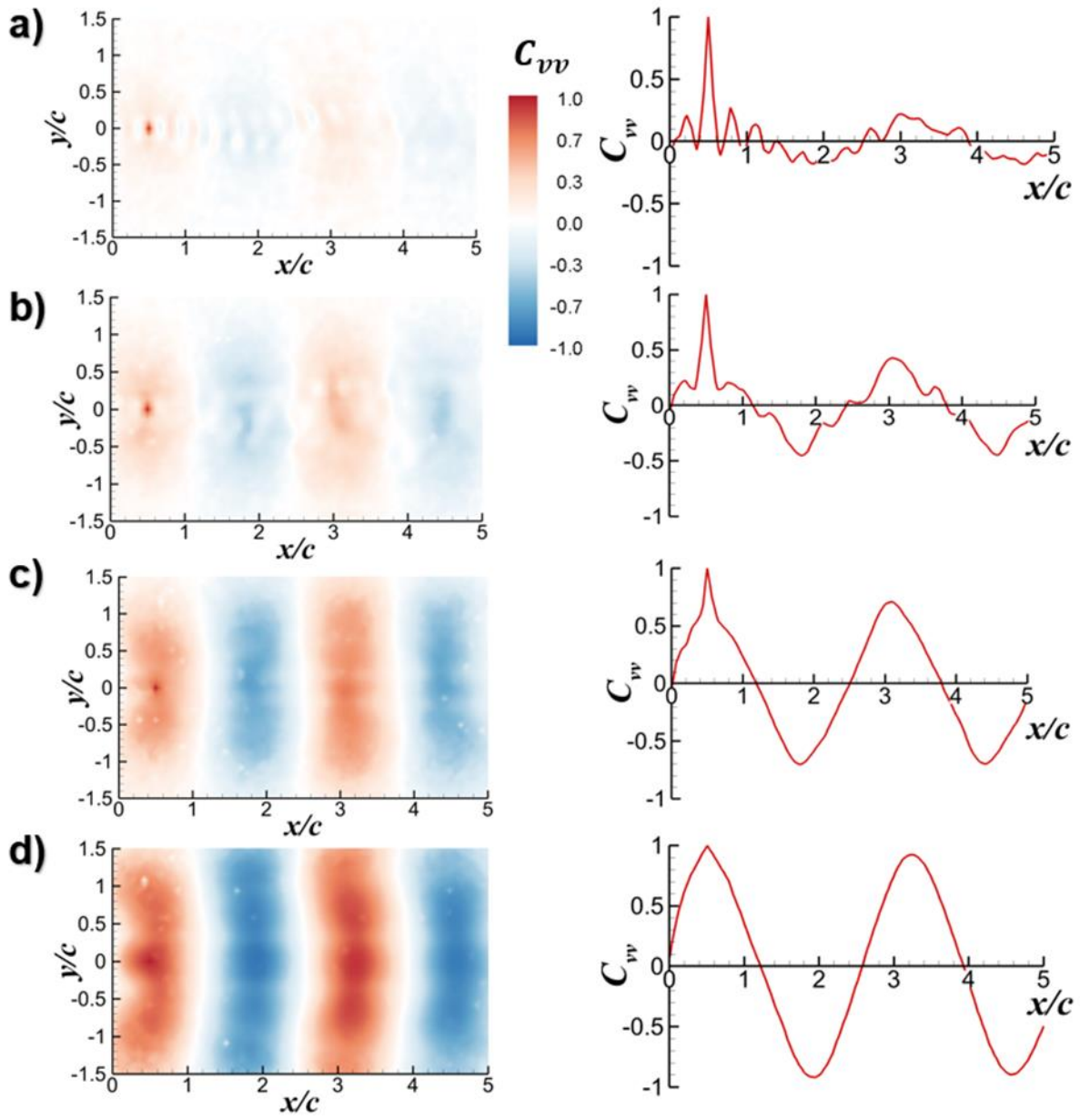

Figure 12 Contours of cross-correlation of cross-stream velocity component C_{vv} (left column); its variation in the streamwise distance at y/c=0 (right column) for k = 1.26 and a) A/c = 0.05, St = 0.02, b) A/c = 0.1, St = 0.04, c) A/c = 0.2, St = 0.08, and d) A/c = 0.4, St = 0.16.

have approximately the same percentage of the total energy for each case (see Figure 13(e)). With increasing amplitude A/c, the spatial structure of the modes changes from an ellipse with major axis in the streamwise direction to one with major axis in the cross-stream direction as the cross-stream extent of the structures increases, while the wavelength remains constant. The relative energy of the first two modes increases with increasing amplitude A/c (and St) at a fixed value of reduced frequency k = 1.26.

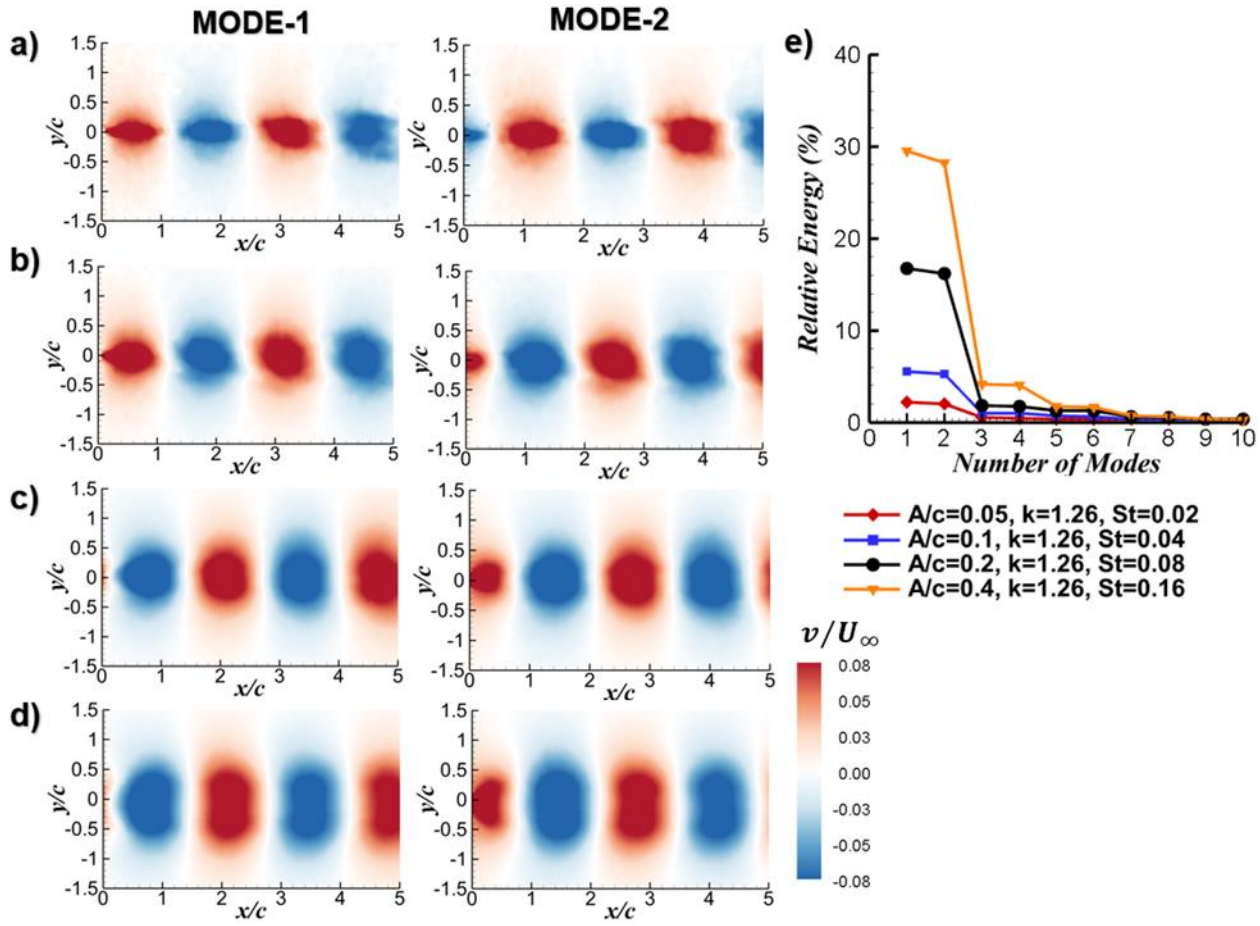

Figure 13 First two POD modes of cross-stream velocity component for k = 1.26 and a) A/c = 0.05, St = 0.02, b) A/c = 0.1, St = 0.04, c) A/c = 0.2, St = 0.08, and d) A/c = 0.4, St = 0.16; e) ratio of the energy of mode to the total energy.

As the first two POD modes represent the fundamental wake mode and have more energy compared to the higher modes, the sum of the energy of the first two modes (E_1+E_2) as a fraction of the total energy E_T, represents the relative contribution of the fundamental wake modes. The quantity (E_1+E_2)/E_T is shown as a function of the reduced frequency k in Figure 14(a) and the Strouhal number St in Figure 14(b). It is seen that the collapse of the data with St is very good. As discussed earlier, the time-averaged quantities such as the mean velocity appears to have a good correlation with St, however the quantity (E_1+E_2)/E_T for the fluctuating field is even better correlated with St. For very small values of St, the percentage energy of the fundamental wake mode behaves like a parabola, but there is a different trend for St > 0.05. We note that the drag force switches to thrust force at approximately $St \approx 0.05$ (see Figure 9(a)). For larger values than 0.05, the percentage energy increases with increasing St, but at a decreasing rate.

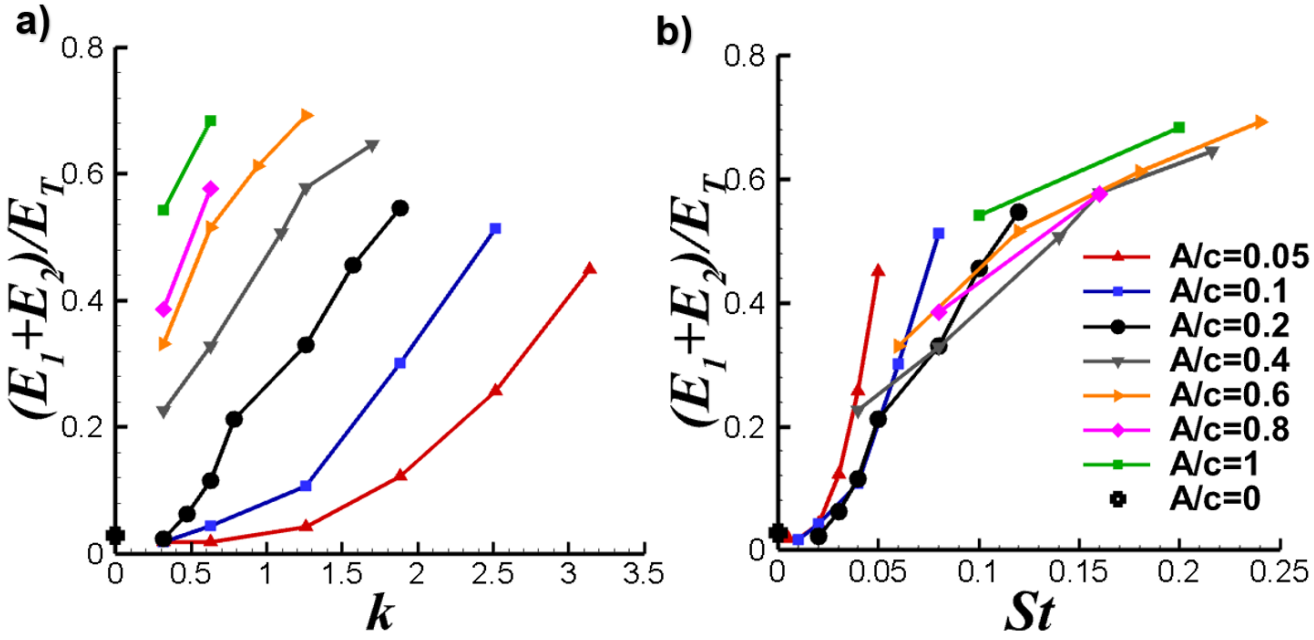

Figure 14 Ratio of the energy of the first two modes to the total energy as a function of a) reduced frequency, b) Strouhal number.

3.3 Coherence of crossflow

We carried out a similar analysis of the cross-correlation coefficient and the POD modes of the cross-stream component in the measurement plane at x/c = 4.03. We present the effects of the reduced frequency k and the Strouhal number St for the same kinematic parameters that were used in previous sections, and then summarize for all cases tested. Figure 15 shows the variation of the normalized rms of the cross-stream component of velocity (left column), the two-point cross-correlation coefficients of the cross-stream velocity component (middle column), and the cross-correlation coefficient C_{vv} (y/c = 0, z/c) along the wake centerline (right column), for the same cases shown in Figure 3. If a 2D vortex filament remains perfectly two-dimensional without any deformation in the spanwise direction, then the cross-correlation coefficient in the spanwise direction is unity.

The variation of the rms cross-stream velocity in the crossflow plane for the stationary airfoil (Figure 15(a)) suggests that it is fairly two-dimensional in the measurement domain. However, we note that this is a time-averaged quantity. When the reduced frequency is increased to k = 0.63 (Figure 15(b)) and k = 1.26 (Figure 15(c)), the rms velocity v_{rms} spreads to a larger area in the cross-stream direction while the maximum value decreases compared to k = 0. For the

largest reduced frequency k = 1.88 (Figure 15(d)), the maximum value substantially increases compared to the other cases. It is noted that only this case has the reverse Karman street configuration (see Figure 3).

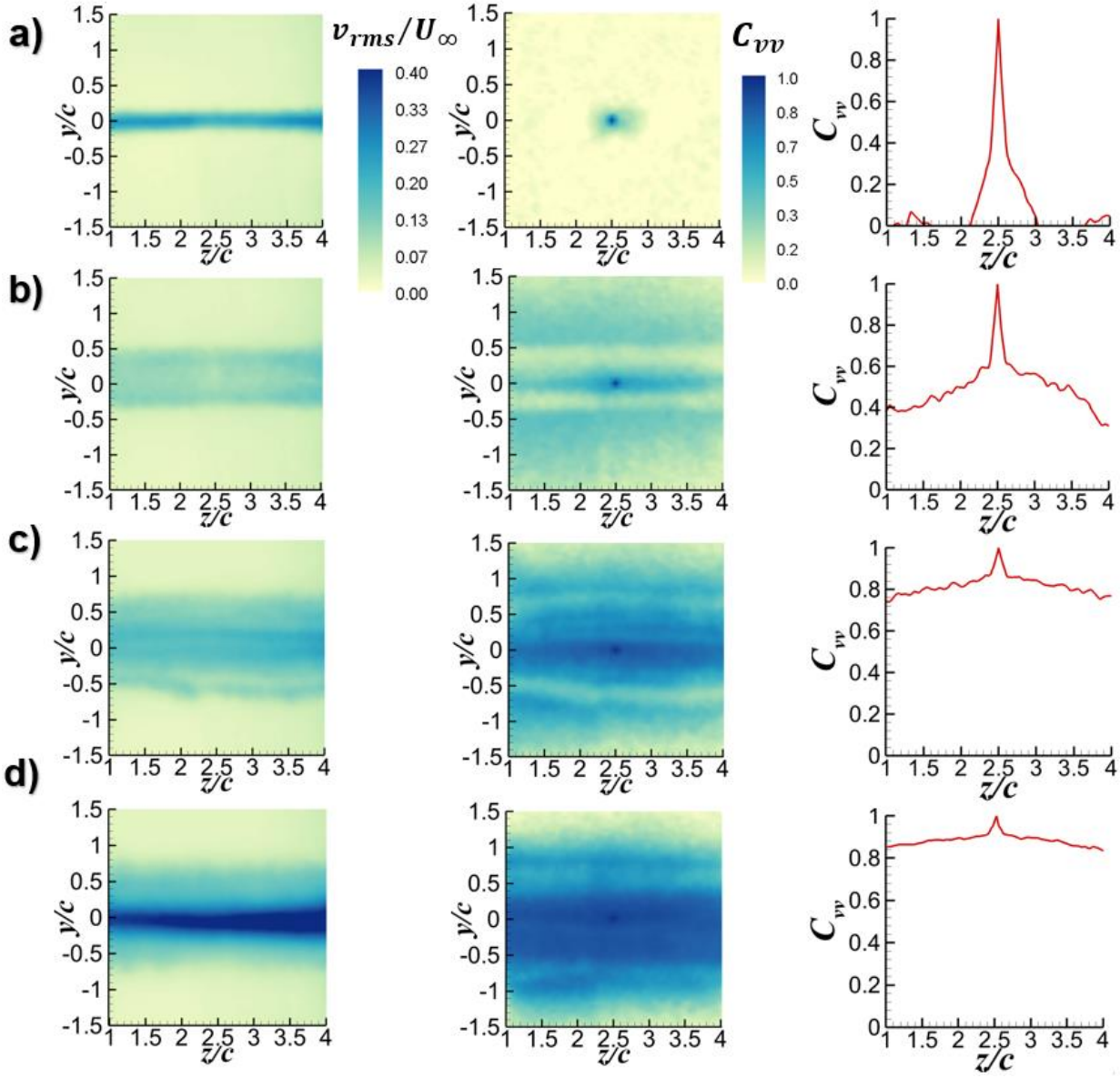

Figure 15 Contour plots of rms cross-stream velocity fluctuations (left column); cross-correlation of cross-stream velocity component (middle column); its variation in the spanwise direction at y/c = 0 (right column) for A/c = 0.1 and a) k = 0, b) k = 0.63, St = 0.02, c) k = 1.26, St = 0.04, and d) k = 1.88, St = 0.06.

Equation (7) shows that the cross-correlation coefficient is obtained by normalizing the cross-correlation with the respective amplitudes at two points. Therefore, it is not affected much by the choice of the reference point as long as the two points are not chosen well outside the wake (in freestream where there are no oscillations of flow). In addition, the reference point in the crossflow plane is chosen as the wake centerline where the velocity fluctuations are very large. The cross-correlation coefficients can be compared for all cases in the middle column. In all cases, the reference point is the center of the wake (y/c = 0, z/c = 2.5) for the two-point cross-correlations. For the stationary airfoil, the cross-correlation contours are roughly circular, but confined to a very small region. In the right column, for the stationary airfoil, the cross-correlation coefficient $C_{vv}(y/c = 0, z/c)$ along the wake centerline reveals that the cross-correlation rapidly decreases with distance from the reference point.

Hayakawa and Hussain (1989) also found no evidence of any periodicity in the spanwise cross-correlations at x/d = 20. They stated that "*the secondary vortices observed by Wei & Smith in the vicinity of the cylinder could not be directly related to apparent substructures recognized by the present measurement* [integral length scale based on the spanwise correlations]." The evidence of the bluff-body wake instabilities are all limited to very near-wake. For example, Wei and Smith (1986) visualised the secondary vortices at a distance less than one diameter; Lin *et al.* (1996) measured the streamwise vorticity concentrations at a distance of one diameter and found spatial periodicity in the spanwise cross-correlation. Our cross-flow plane of the measurements is at x/c = 4.03, which corresponds to approximately 34 times the thickness of the airfoil (and 269 times the local momentum thickness) at a chord Reynolds number of 20,000.

Using the information shown in Figure 15, one can obtain an estimate of the spanwise length-scale L defined as:

$$L/c = \int_{\frac{z}{c}=1}^{\frac{z}{c}=4} C_{vv}\left(\frac{y}{c}=0, \frac{z}{c}\right) \mathrm{d}\left(\frac{z}{c}\right) \tag{12}$$

For the stationary airfoil, we found $L/c \approx 0.16$, which is on the order of the airfoil thickness and in agreement with measurements in the near-wake of bluff bodies discussed in Section 1.3. Hayakawa and Hussain (1989) reported a spanwise length scale based on the cross-correlation

$L \approx 1.8d$, which is comparable to our finding of $L = 0.16c$ (or 1.33 times the thickness of the airfoil). With increasing reduced frequency in Figure 15, the cross-correlation of the cross-stream velocity fluctuations improve substantially in the crossflow plane (middle column). The cross-correlation coefficient C_{vv} ($y/c = 0$, z/c) in the spanwise direction presented in the right column reveals that the cross-correlation quickly decreases to a background level, which is not zero and increases with increasing reduced frequency. This is qualitatively similar to the findings of Bearman (1984). Figure 7 in Bearman (1984) shows that even the cross-correlation of the surface pressure fluctuations does not exhibit any periodicity in the spanwise direction. The correlation levels increase with oscillation frequency, and reach maximum when the natural vortex shedding frequency is approached. This suggests that the wake instability (vortex shedding) is dominant compared to any secondary instabilities. We note that, for the cases of $k \neq 0$, the definition of the spanwise length-scale given above is not as meaningful. For these cases, we will define the average cross-correlation in the measurement domain and discuss later.

Figure 16(a)-(d) present the first dominant POD mode of the cross-stream velocity component in the crossflow plane for the same cases shown in Figure 15. The first mode has the most energy compared to all other higher modes as revealed in Figure 16(e). Only for $k = 0$, the first mode can be interpreted as a spanwise standing wave with the wavelength to be half of the measurement width. However, the energy of this mode is an extremely small fraction of the total energy. For all $k \neq 0$ cases, the first POD mode can be described as a "flapping mode", which can reach nearly 60% of the total energy at $k = 1.88$.

In order to present the effects of amplitude A/c at a fixed reduced frequency $k = 1.26$, Figure 17 shows the variation of the normalized rms of the cross-stream component of velocity (left column), the two-point cross-correlation coefficients of the cross-stream velocity component (middle column), and the cross-correlation coefficient $C_{vv}(y/c = 0, z/c)$ as a function of spanwise distance (right column), for the same cases presented in Figure 4. The rms cross-stream velocity is approximately uniform in the spanwise direction, and exhibits well defined double-peaks with increasing amplitude A/c, with increasing peak values.

The cross-correlation coefficient shown in the middle column of Figure 17 reveals that the values away from the reference point increase with increasing amplitude A/c, and also spread

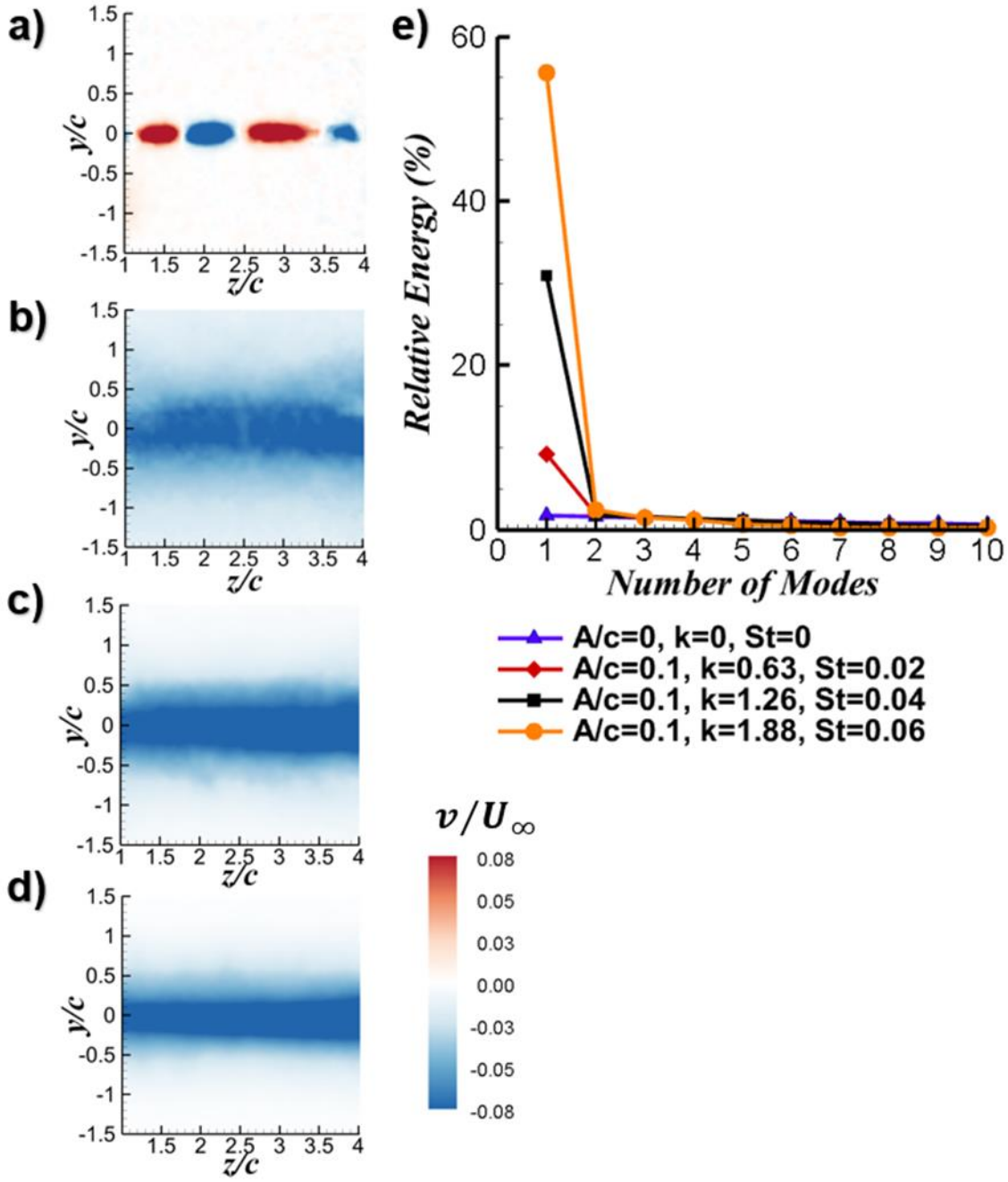

Figure 16 First POD mode of cross-stream velocity component for *A/c* = 0.1 and a) *k* = 0, b) *k* = 0.63, *St* = 0.02, c) *k* = 1.26, *St* = 0.04, d) *k* = 1.88, *St* = 0.06; e) ratio of the energy of mode to the total energy.

to a larger area in the cross-stream direction. The variation of the spanwise cross-correlation shown in the right column reveals that the background cross-correlation at one chord length away from the reference point increases in value around 0.4 to roughly 0.9 with increasing

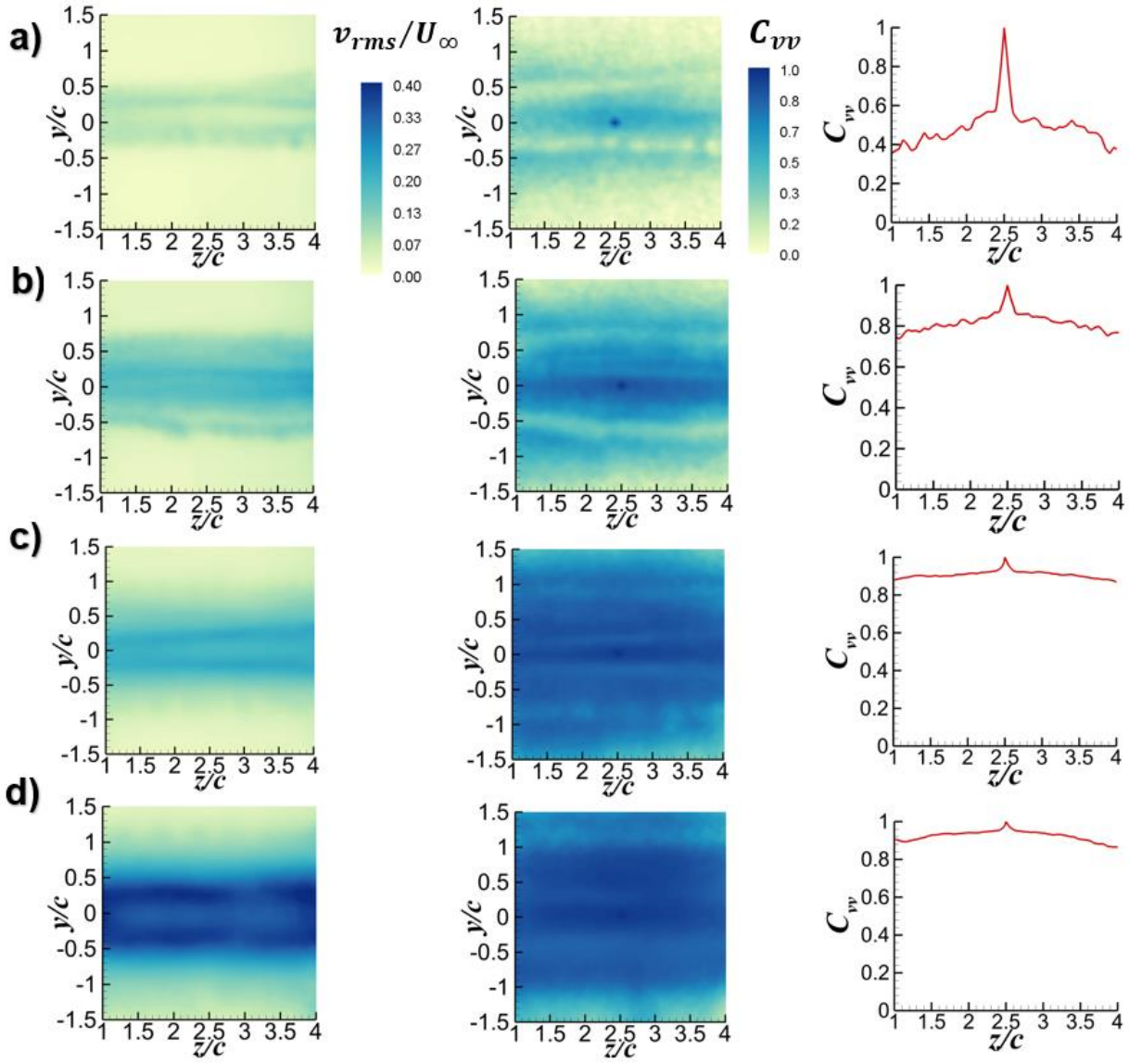

Figure 17 Contour plots of rms cross-stream velocity fluctuations (left column); cross-correlation of cross-stream velocity component (middle column); its variation in the spanwise direction at $y/c = 0$ (right column) for $k = 1.26$ and a) $A/c = 0.05$, $St = 0.02$, b) $A/c = 0.1$, $St = 0.04$, c) $A/c = 0.2$, $St = 0.08$, and d) $A/c = 0.4$, $St = 0.16$.

amplitude A/c. The increasing cross-correlation with increasing amplitude A/c is consistent with the POD analysis shown in Figure 18. In all cases, the first mode is the only dominant mode. The percentage energy of the "flapping mode" increases while its cross-stream extent grows with increasing amplitude A/c. For the largest amplitude, the single flapping mode has around 65% of the total energy of the oscillating wake.

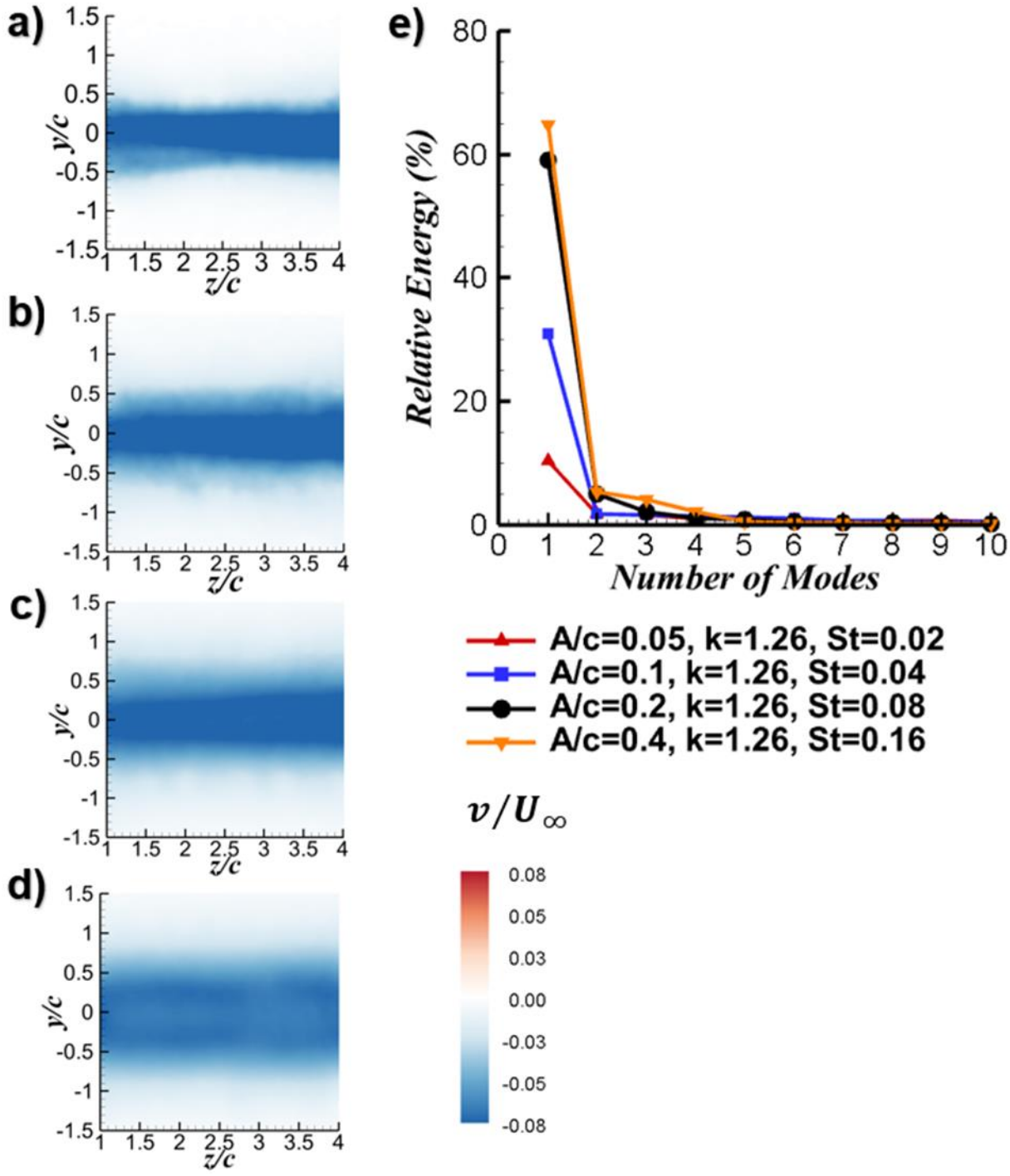

Figure 18 First POD mode of cross-stream velocity component for k = 1.26 and a) A/c = 0.05, St = 0.02, b) A/c = 0.1, St = 0.04, c) A/c = 0.2, St = 0.08 and d) A/c = 0.4, St = 0.16; e) ratio of the energy of mode to the total energy.

As the flapping mode has most of the energy of the oscillating wake in the crossflow plane, we plot the ratio of the first mode energy to the total energy, E_1 / E_T, as a function of the reduced frequency k in Figure 19(a) and the Strouhal number St in Figure 19(b) for all cases tested. The

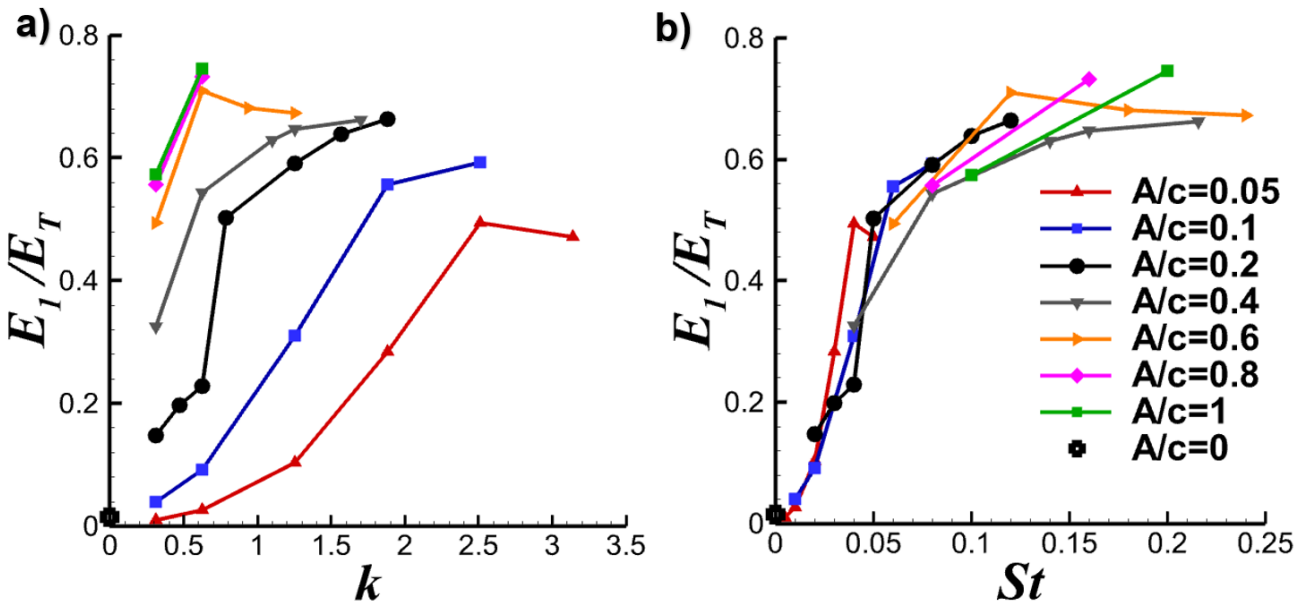

Figure 19 Ratio of the energy of the first mode to the total energy as a function of a) reduced frequency, b) Strouhal number.

collapse of the data for the crossflow with *St* is even better than that displayed in Figure 14(b) for the streamwise flow. There are also similar regimes for small *St* in the drag-producing flows, in which the energy percentage of the first mode behaves like a parabola, and for large *St* in the thrust-producing flows, in which it behaves like an exponential curve with negative exponent. The border between the two regions, which is around $St \approx 0.05$, corresponds to the net zero force for the oscillating wake.

Previously we discussed the spanwise length-scale using the integral of the cross-correlation coefficient in the spanwise direction for the stationary airfoil. This definition, if applied to the other cases ($k \neq 0$), would be dependent on the width of the measurement domain. (For example, $L = 3c$ for the perfectly correlated hypothetical case as the width of the measurement domain is $3c$). Instead, we define the average cross-correlation over the total width of $3c$ as:

$$C_{vv,ave} = \frac{1}{3}\int_{\frac{z}{c}=1}^{\frac{z}{c}=4} C_{vv}\left(\frac{y}{c}=0,\frac{z}{c}\right)\mathrm{d}\left(\frac{z}{c}\right) \tag{13}$$

The variation of the average cross-correlation coefficient in the measurement domain is shown as a function of the reduced frequency *k* in Figure 20(a) and the Strouhal number *St* in Figure 20(b). Again, we see a very good correlation with the Strouhal number *St*, which may be expected based on the good correlation with the percentage of energy of the dominant POD mode shown in Figure 19(b) previously. For the spanwise averaged cross-correlation coefficient shown in Figure 20(b), we identify two regions: for small *St*, there is a rapid increase with *St*, which is similar to a steep parabola (similar to Figures 14(b) and Figure 19(b)), but can be approximated as a linear curve:

$$C_{vv,ave} = 20\,St \tag{14}$$

In the second region, for larger St, the spanwise averaged cross-correlation coefficient is roughly constant:

$$C_{vv,ave} \approx 0.92 \tag{15}$$

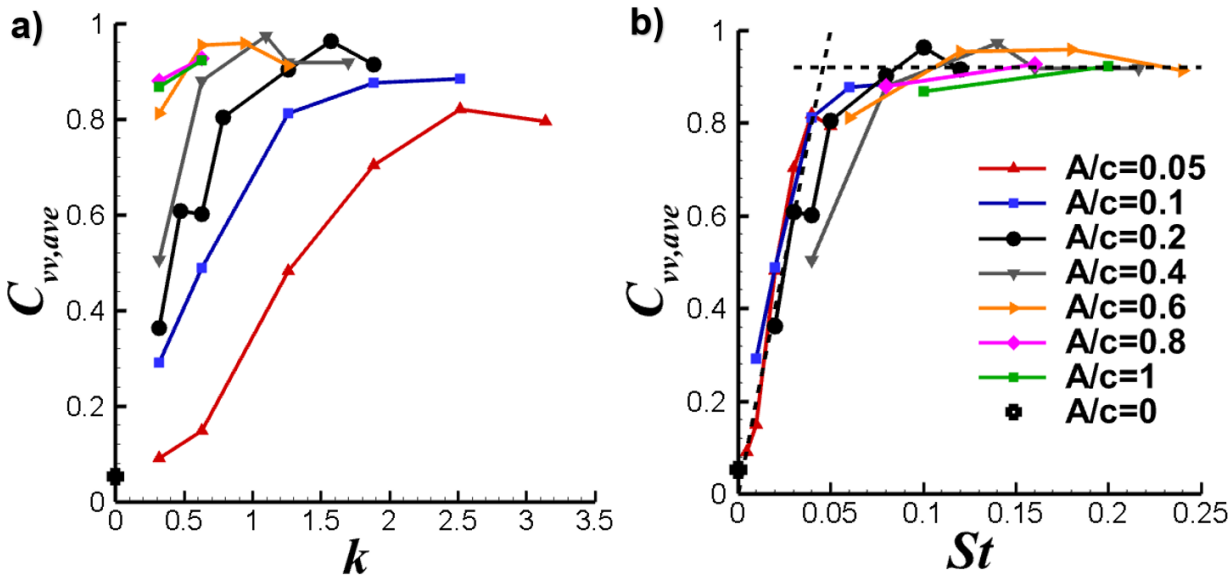

Figure 20 Spanwise-averaged cross-correlation at *y/c* = 0 as a function of a) reduced frequency and b) Strouhal number. Dashed lines indicate curve fits for small and large Strouhal numbers.

We note that, if there were no small-scale turbulence and the flow were purely two-dimensional, the spanwise-averaged cross-correlation coefficient would be unity. The case of perfect cross-correlation in the spanwise direction (two-dimensional flow and independent of

z) also corresponds to the existence of only one mode in the Proper Orthogonal Decomposition, if Equation (6) is adapted for the cross-flow. This can be shown directly by using the definitions in Equations (6) and (7). In general, dominant modes with higher energy fraction and larger spatial POD mode correspond to higher mean correlation in the spanwise direction. In our measurements, the spanwise-averaged cross-correlation is not unity, but around 0.92 due to the small-scale turbulence in the vortical flow. The forms of Equations (14) and (15) were chosen as the simplest cases as well as to emphasise the different regions of Strouhal number. The two curves for the two regions intersect at around $St \approx 0.05$, which is the border between the drag and thrust forces. As the thrust force is generally associated with the reverse Karman vortex street composed by rolled-up vortices, it appears that spanwise vortices generated in this regime are expected to be highly two-dimensional.

We note that, in our experiments, we measured a weak spanwise velocity component (on the order of 10% of the freestream velocity) in some cases, however it is difficult to draw any conclusions about the spanwise flow in the vortex core from the measurements at a fixed cross-flow plane at four chord length downstream. As the flow is not fully coherent, especially at low Strouhal numbers, the deformation of the vortex filament in the spanwise direction and the resulting curvature of the vortex axis can also lead to the appearance of the spanwise velocity component. Even though the rms velocity in the spanwise direction is nearly uniform, spanwise vortices are not truly two-dimensional. It is more prudent to say that spanwise vortices are quasi-two-dimensional at high Strouhal numbers.

3.4 Implications of spanwise coherence

As discussed in the Introduction (Section 1.4), oscillating wakes are commonly used as gust generators in various experimental simulations. The present study, although limited to the pure plunging motion, gives some insight to the degree of the two-dimensionality of the oscillating wakes. Experimentally generated gusts, wakes, and vortices may exhibit specific characteristics while the essential aspects, including the vorticity shedding, roll up, and spanwise vortices, are expected to have some commonality. Based on our study, we predict that unsteady wakes can be assumed to be approximately two-dimensional if the Strouhal number *St*, which is an amplitude parameter, is larger than a critical value. For smaller Strouhal numbers, the average cross-correlation increases with increasing Strouhal number (wake or

gust amplitude). In our case of plunging airfoils, the critical value of the Strouhal number is approximately $St \approx 0.05$. This corresponds to a ratio of the maximum plunge velocity to the freestream velocity of approximately 0.16 and $\alpha_{eff,max} \approx 9°$. It is also seen in Figure 7(b) that $v_{rms,max}/U_\infty$ is generally less than 0.1, if the Strouhal numbers are less than 0.05. If the maximum wake angle is taken as a rough approximation to the gust angle generated by the wake, it corresponds to a gust amplitude of approximately 6° for the pure plunging motion. This value could be an upper limit for experimentally generated small-amplitude gusts. This rough estimate can also be used for other airfoil motions (pure pitching and combined pitching and plunging), if the generalized Strouhal number based on the total excursion of the trailing-edge of the airfoil is used (Triantafyllou *et al*. 1991; Anderson *et al*. 1998). In summary, in our case, if wakes of plunging airfoils are to be used as gust generators to produce small-amplitude gusts, the wakes need to operate at $St \leq 0.05$. Unfortunately, in this range of the Strouhal numbers, the unsteady wake can be far from being two-dimensional.

The decay of the vorticity in the streamwise direction may cause a nonuniform variation in the amplitude of the travelling-wave gusts in this kind of gust generators. We believe that this is a secondary level effect compared to the lack of spanwise coherence, and may be alleviated to a certain extent by choosing the ratio of the chord-length to the gust wavelength to be small. Lack of two-dimensionality is expected to decrease the magnitude of the unsteady forces acting on downstream bodies. In the simplest two-dimensional aerodynamic model, the instantaneous lift is proportional to the instantaneous cross-stream velocity, with a well-known frequency correction for attached flows (Theodorsen, 1935). The amplitude of the lift fluctuations is given by:

$$c_l = 2\pi \frac{v}{U_\infty} \left(\boldsymbol{C}(k) + i\frac{k}{2} \right) \tag{16}$$

where the Theodorsen function $\boldsymbol{C}(k)$ is a complex number and i is the imaginary unit. This two-dimensional attached flow model can be extended to the three-dimensional wings, by including the two-point cross-correlation coefficients of the cross-stream velocity fluctuations. The physical basis of including cross-correlations in the spanwise direction comes from the use of the strip-theory. Massaro and Graham (2015) and others cited in their paper used this approach in which the two-dimensional lift is integrated over the span to compute the total lift on the whole span. In our case, their approach can be applied by integrating the sectional lift while also taking into account the cross-correlations of the cross-stream velocity:

$$C_L = \frac{1}{b}\int 2\pi\, C_{vv}\frac{v}{U_\infty}\left(\boldsymbol{C}(k) + i\frac{k}{2}\right)dz \tag{17}$$

where *b* is the span of the wing. Therefore, for a rectangular wing and uniform velocity in the spanwise direction, we predict that the ratio of the lift fluctuations is given by the spanwise-averaged cross-correlation:

$$\frac{C_L}{c_l} = \frac{1}{b}\int C_{vv}\, dz = C_{vv,ave} \tag{18}$$

It appears that this may be a more important issue for the experimental simulation of small-amplitude gusts for which the amplitude of wake excitation (*St* in our case) is also small and the wake is far from being nearly two-dimensional. For small *St*, the spanwise-averaged cross-correlation increased linearly for our experiments.

To support our argument, we present the results from various experimental facilities and compare different methods of gust generation and unsteady wing motion. When unsteady lift of an airfoil submerged in the wake flows is considered, the parameter *k* is the only parameter for small-amplitude disturbances in the Theodorsen and Sears formulations. Figure 21 is a typical plot commonly used to present the experimental lift data obtained in various gust generators. The different red symbols in Figure 21 show the ratio of the amplitude of the unsteady lift force to that of the quasi-steady lift force, $L_{amp}/L_{qs,amp}$, as a function of the reduced frequency *k* from previous studies (Cordes et al. 2017; Wei *et al.* 2019b; Wu *et al.* 2020), in which cascades of oscillating airfoils are used to generate travelling-wave gusts. The data cover a range of gust amplitudes, Reynolds numbers, and airfoil profiles, but in all cases it is believed that (mostly) attached flows are maintained. The solid red line shows the Sears (1941) solution, which has good agreement with the experiments at higher *k*, but both the deviation from the theory and scatter of the data significantly increase at low reduced frequencies.

The discrepancy of the data of Cordes *et al.* (2017) with the Sears function at low reduced frequencies was attributed to various factors. Cordes *et al.* (2017) suggested that the experimental results show good agreement with the Atassi theory, which takes into account the distortion of the steady velocity field by the presence of an airfoil. Wei *et al.* (2019b) attributed

the discrepancy to the turbulent wakes causing large intermittent peaks in the gust angle. They also reported that the two-dimensional simulations agree with the experiments in the low reduced-frequency region over which the potential flow results are very different. The two-dimensional numerical simulations cannot take the spanwise coherence into account. This remains as an open question. In addition, it is not clear how the turbulent wake from an upstream gust generator causes very large discrepancy from the theory at low frequencies, but still provides excellent agreement at higher frequencies. Wu *et al.* (2020) suggested that, in addition to the "highly turbulent wakes", there is a second flow mechanism which contributes to this discrepancy at low reduced frequencies. They proposed that the existence of the airfoil in the test section may impact the gust angle. It is likely that the spanwise coherence of the oscillating wakes in these gust generators is far from being two-dimensional in this range. In contrast, the blue triangular symbols, which show the results for a standing-wave type of gust generator (Fernandez *et al*. 2021), reveal very good agreement with the corresponding theoretical solution of Theodorsen (1935). This particular standing-wave gust generator relies on the periodic deflection of freestream rather than oscillating wakes with travelling waves, and believed to have better two-dimensionality of the gusts generated. It is noteworthy that, even at very low reduced frequencies, the agreement with the theory is very good. This shows that, excellent agreement with the theory exists, if the wake flows are not used as gust generators.

The plunging airfoil case is identical to a fixed airfoil in standing-wave gusts. The blue square symbols in Figure 21 show the case of plunging airfoil (Chiereghin et al. 2019), which also reveal good agreement with the Theodorsen theory. The difference between the Theodorsen and Sears solutions for $k \leq 0.25$ is negligible, yet the experimental data for the standing-wave gusts and travelling-wave gusts exhibit very large deviations from each other. Physically we expect that, at the very long wavelength limit (very small k), both the travelling-wave and standing-wave gusts should produce similar lift response, just like the Theodorsen and Sears solutions merge. Our experiments suggest that the source of this discrepancy in the measured lift response of fixed airfoils in travelling-wave and standing-wave gusts may be due to the differences in the spanwise coherence of the simulated gusts. Unfortunately, measurements of the spanwise coherence of the experimentally produced gusts have been lacking in the literature. Our findings in this paper point out the importance of this long-neglected issue.

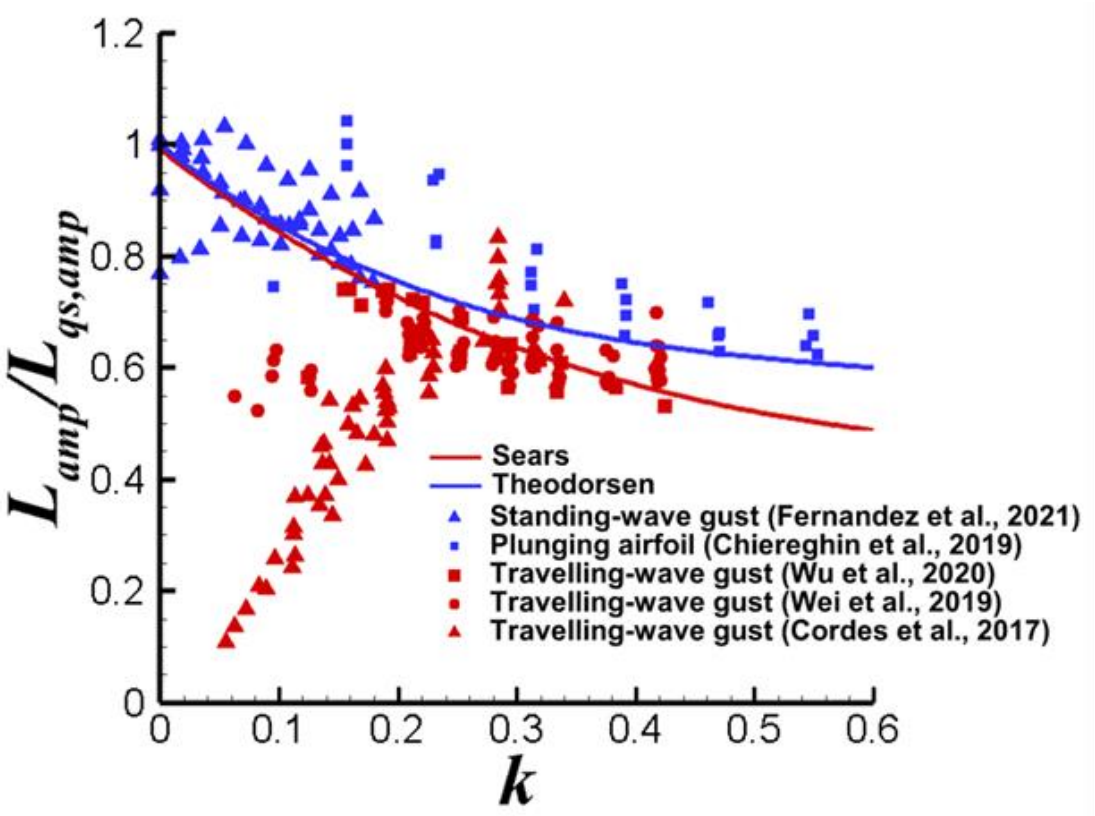

Figure 21 Ratio of the amplitude of lift to that of quasi-steady lift from literature for travelling-wave gusts, standing-wave gusts, plunging airfoils, the Sears and Theodorsen predictions.

4. Conclusions

The unsteady wakes of a periodically plunging airfoil set at zero mean angle of attack at a chord Reynolds number of Re = 20,000 were investigated by means of particle image velocimetry measurements. The main focus was to understand the effect of the main parameters, which are the reduced frequency k and the Strouhal number St based on the peak-to-peak plunge amplitude, on the unsteady characteristics and coherence of the oscillating wakes. The measurements of streamwise flow and crossflow in the near-wake were analysed using two-point cross-correlations and the Proper Orthogonal Decomposition of the oscillating wakes for a wide range of parameters ($k \leq 3.14$ and $St \leq 0.24$).

The instantaneous vortical flow in the near wake appears as a travelling wave with much larger amplitude than the amplitude of the airfoil motion at low Strouhal numbers. The peak-to-peak amplitude of the travelling wave is more dependent on the reduced frequency. With increasing

Strouhal number, a reverse Karman vortex street configuration with relatively smaller spacing between the two rows is observed. Within the range of kinematic parameters tested, the mean streamwise velocity at the centerline generally increases with increasing k and A/c. There is a better trend of the data to collapse with St than k, except for higher frequencies at each fixed amplitude A/c. Similarly, the maximum rms velocity fluctuations exhibit better collapse with St than k, particularly at lower values of k. The degree of the collapse in the whole range of the data significantly increases for the momentum thickness and the corrected thrust coefficient. Estimates of the thrust coefficient using the method of Bohl and Koochesfahani (2009) suggest that drag force switches to thrust force at approximately $St \approx 0.05$ at this Reynolds number. Our data for the whole range of the parameters tested confirm the significant effect of the reduced frequency on the time-averaged thrust coefficient. The dependence on the reduced frequency can be represented by the same function proposed by Garrick (1936), but multiplied by a 26% smaller constant. We suggest that this correction represents the roll-up of vortex sheets instead of remaining planar as assumed by the Garrick theory.

With increasing frequency and amplitude of the airfoil motion, the peak cross-correlation coefficient of the streamwise flow in the near-wake increases. We find qualitative similarities with the wake synchronisation and vortex lock-in of oscillating bodies and airfoils. The streamwise flow is characterized by the first two POD modes, which are the fundamental wake modes and describe a travelling wave. The relative energy of the first two modes increases with increasing frequency and amplitude of the airfoil motion. The relative contribution of the fundamental wake modes, $(E_1+E_2)/E_T$, has much better correlation with St than the time-averaged quantities of the flow. For drag producing wakes, the percentage energy of the fundamental wake modes increases rapidly with increasing Strouhal number. In contrast, it increases more slowly for thrust producing wakes.

The crossflow measurements in the near-wake revealed that, although the rms cross-stream velocity fluctuations are uniform in the spanwise direction, the two-point cross-correlation coefficient decays rapidly for the stationary airfoil ($k = 0$). The spanwise length scale for this case drops to around $L \approx 0.16c$ at $x/c = 4.03$, which is on the order of the airfoil thickness. With increasing frequency and amplitude of the airfoil oscillations, while the rms velocity fluctuations remain nearly uniform, the cross-correlation coefficient drops rapidly with spanwise distance from the reference point (wake centerline at the mid-span) to a nearly

constant level. This constant level of the cross-correlation coefficient increases with increasing reduced frequency and Strouhal number. The corresponding POD analysis of the cross-stream velocity fluctuations show that there is only a single dominant mode for the oscillating wakes, which can be described as a "flapping mode". The ratio of the energy of the first mode energy to the total energy, E_1 / E_T, shows very good correlation with Strouhal number, exhibiting different behaviour in drag producing and thrust producing wakes. The spanwise-averaged cross-correlation coefficient in the measurement domain again reveals a very good correlation with the Strouhal number *St*, consistent with the good correlation of the percentage energy of the dominant POD mode. Two regions are identified as a function of Strouhal number. For small *St*, the spanwise-averaged cross-correlation coefficient grows almost linearly in the drag producing region. For larger *St* in the thrust producing region, the spanwise averaged cross-correlation coefficient is roughly constant ($C_{vv,ave} \approx 0.92$). This high value of the cross-correlation suggests highly two-dimensional spanwise vortices in the thrust producing regime for $x/c \leq 4$ at $Re = 20{,}000$.

In summary, we compared the effects of the reduced frequency and the Strouhal number on various flow quantities, including the mean streamwise velocity, the maximum rms velocity, momentum thickness, mean thrust, energy percentage of the dominant POD modes, and the spanwise-averaged cross-correlation coefficient. In all cases, it was shown that the Strouhal number was the more dominant parameter. The Strouhal number represents the amplitude parameter for the excitation of the wake. Once it reaches a sufficient amplitude, the unsteady wake becomes more synchronized. The observed saturation of the mode energies and the spanwise-averaged cross-correlation for $St \geq 0.05$ is due to the wake synchronization. The threshold value of $St \approx 0.05$ was consistent with previous numerical simulations of the unsteady wakes. Once the wake becomes synchronized, further increase in the amplitude does not increase the coherence of the flow.

Finally, the implication of the lack of two dimensionality was discussed for gust generators that are based on oscillating airfoils. While our study is limited to plunging airfoils, it suggests that the Strouhal number based on the plunge amplitude, which is also a measure of the gust amplitude produced in the wake, is the most important parameter that determines the degree of two-dimensionality. For small gust angles we may expect less two dimensionality, and smaller lift force fluctuations on downstream wings. This may necessitate corrections of the measured

lift amplitude, using two-point cross-correlations of the gust angle. For a simple aerodynamic model in which the lift fluctuations are proportional to the amplitude of the gust angle, it is shown that the correction can be achieved by the use of the spanwise-averaged cross-correlation of gust angle. The comparison of the experimental results obtained using travelling-wave gusts, standing-wave gusts, and plunging airfoils reveals that there exists a large scatter of data as well as deviations from the theory only for the travelling-wave gusts. This implies that travelling-wave gusts may be far from being two-dimensional in some cases. We suggest that the spanwise coherence of the experimentally produced gusts should be considered when interpreting the amplitude of the lift fluctuations on downstream wings.

Acknowledgments

The authors would like to acknowledge the Engineering and Physical Sciences Research Council (EPSRC) Grant No. EP/S028994/1, the EPSRC strategic equipment Grant (EP/K040391/1) that made the velocity measurements possible, and the Republic of Turkey Ministry of National Education Scholarship for the first author.

REFERENCES

ANDERSON, J., STREITLIEN, K., BARRETT, D., & TRIANTAFYLLOU, M., 1998, Oscillating foils of high propulsive efficiency, *Journal of Fluid Mechanics*, **360**, 41-72.

BEARMAN, P. W. 1984 Vortex shedding from oscillating bluff-bodies, *Annual Review of Fluid Mechanics*, **16**, pp. 195-222.

BENDAT, J. AND PIERSOL, A. 1986 *Random data analysis and measurement procedures*. Hoboken.

BERKOOZ, G., HOLMES, P. AND LUMLEY, J. L. 1993 The proper orthogonal decomposition in the analysis of turbulent flows, *Annual Review of Fluid Mechanics*, **25**, pp. 539-575.

BERNAL, L. P. AND ROSHKO, A. 1986 Streamwise vortex structure in plane mixing layers, *J. Fluid Mechanics*, **170**, pp. 499-525.

BICKNELL, J. AND PARKER, A. G. 1972 A wind-tunnel stream oscillation apparatus, *Journal Aircraft*, **9** (6), pp. 446–447.

BOHL, D. G. AND KOOCHESFAHANI, M. M. 2009 MTV measurements of the vortical field in the wake of an airfoil oscillating at high reduced frequency, *J. Fluid Mechanics*, **620**, pp. 63-88.

BOOTH, E. R. AND YU, J. C. 1986 Two-dimensional blade-vortex flow visualization investigation, *AIAA J.*, **24** (9), pp. 1468–1473.

BRION, V., LEPAGE, A., AMOSSE, Y., SOULEVANT, D., SENECAT, P., ABART, J. C. AND PAILLART, P. 2015 Generation of vertical gusts in a transonic wind tunnel, *Exp. Fluids*, **56**.

BUCHNER, A.J., BUCHMANN, N. & KILANY, K., ATKINSON, C. & SORIA, J. 2012 Stereoscopic and tomographic PIV of a pitching plate. *Exp Fluids* **52,** 299–314.

CALDERON, D. E., CLEAVER, D. J., GURSUL, I. AND WANG, Z. 2014 On the absence of asymmetric wakes for periodically plunging finite wings, *Physics of Fluids*, **26** (7).

CHARONKO, J. J. AND VLACHOS, P. P. 2013 Estimation of uncertainty bounds for individual particle image velocimetry measurements from cross-correlation peak ratio, *Measurement Science and Technology*, **24** (6).

CHIEREGHIN, N., BULL, S., CLEAVER, D. J. AND GURSUL, I. 2020 Three-dimensionality of leading-edge vortices on high aspect ratio plunging wings, *Physical Review Fluids*, **5** (6).

CHIEREGHIN, N., CLEAVER, D. J. AND GURSUL, I. 2019 Unsteady lift and moment of a periodically plunging airfoil, *AIAA J.*, **57** (1), pp. 208-222.

CLEAVER, D. J., CALDERON, D. E., WANG, Z. AND GURSUL, I. 2013 Periodically plunging foil near a free surface, *Exp. Fluids*, **54** (3).

CLEAVER, D. J., WANG, Z., GURSUL, I. AND VISBAL, M. R. 2011 Lift enhancement by means of small-amplitude airfoil oscillations at low Reynolds numbers, *AAIA J.*, **49** (9), pp. 2018-2033.

CORDES, U., KAMPES, G., MEISSNER, T., TROPEA, C., PEINKE, J. AND HOLLING, M. 2017 Note on the limitations of the Theodorsen and Sears functions, *J. Fluid Mechanics*, **811**.

DAVID, L., JARDIN, T., BRAUD, P. & FARCY, A. 2012 Time-resolved scanning tomography PIV measurements around a flapping wing. *Exp Fluids* **52,** 857–864.

EKATERINARIS, J. AND PLATZER, M. 1998 Computational prediction of airfoil dynamic stall, *Progress in Aerospace Sciences*, **33**, pp. 759–846.

FERNANDEZ, F., CLEAVER, D. AND GURSUL, I. 2021 Unsteady aerodynamics of a wing in a novel small-amplitude transverse gust generator, *Exp. Fluids*, **62**.

GAO, A., SHERWIN, S. J. AND CANTWELL, C. D. 2020 Three-dimensional instabilities of vortices shed from a plunging wing: Computations, *Bulletin of the American Physical Society*, the 73rd Annual Meeting of the APS Division of Fluid Dynamics (APS DFD 2020), 22-24 November 2020, virtual meeting.

GARRICK, I. E. 1936 Propulsion of a flapping and oscillating airfoil, *NACA Tech. Rep. 567.*

GILMAN, J. AND BENNETT, R. M. 1966 Wind-tunnel technique for measuring frequency-response functions for gust load analyses, *Journal Aircraft*, **3** (6), pp. 535–540.

GURSUL, I. AND CLEAVERS, D. 2019 Plunging oscillations of airfoils and wings: progress, opportunities, and challenges, *AAIA J.*, **57** (9), pp. 3648-3665.

HAYAKAWA, M. AND HUSSAIN, F. 1989 Three-dimensionality of organized structures in a plane turbulent wake, *J. Fluid Mechanics*, **206**, pp. 375-404.

HEATHCOTE, S., WANG, Z. AND GURSUL, I. 2008 Effect of spanwise flexibility on flapping wing propulsion, *J. Fluids Struct.*, **24** (2), pp. 183-199.

HEATHCOTE, S. F. 2006 Flexible flapping airfoil propulsion at low Reynolds numbers. PhD thesis. The University of Bath.

HEILAND, R. W. 1992 KLTOOL: a mathematical tool for analyzing spatiotemporal data. PhD thesis. Arizona State University.

JONES, W. P. AND MOORE, J. A. 1972 Flow in the wake of a cascade of oscillating airfoils, *AAIA J.*, **10** (12), pp. 1600–1605.

KARNIADAKIS, G.E. & TRIANTAFYLLOUS, G.S., 1989 Frequency selection and asymptotic states in laminar wakes, *Journal of Fluid Mechanics*, **199**, pp. 441-469.

KOOCHESFAHANI, M. M. 1989 Vortical patterns in the wake of an oscillating airfoil, *AAIA J.*, **27** (9), pp. 1200-1205.

LIN, J.C., VOROBIEFF, P. & ROCKWELL, D., 1996 Space–time imaging of a turbulent near-wake by high-image-density particle image cinematography, *Physics of Fluids*, **8**, pp. 555-564.

MASSARO, M. AND GRAHAM, J. M. R. 2015 The effect of three-dimensionality on the aerodynamic admittance of thin sections in free stream turbulence, *Journal of Fluids and Structures*, **57**, pp. 81-90.

MCCROSKEY, W. J. 1982 Unsteady airfoils, *Annual Review of Fluid Mechanics*, **14** (1), pp. 285-311.

SEARS, W. R. 1941 Some aspects of non-stationary airfoil theory and its practical application, *J. Aeronaut. Sci.*, **8** (3), pp. 104-108.

SHYY, W., AONO, H., CHIMAKURTHI, S. K., TRIZILA, P., KANG, C. K., CESNIK, C. E. S. AND LIU, H. 2010 Recent progress in flapping wing aerodynamics and aeroelasticity, *Progress in Aerospace Sciences*, **46** (7), pp. 284-327.

SIROVICH, L. 1987 Turbulence and the dynamics of coherent structures part i: coherent structures, *Quarterly of Applied Mathematics*, pp. 257-267.

SMITS, A. J. 2019 Undulatory and oscillatory swimming, *J. Fluid Mechanics*, **874**.

SON, O., WANG, Z. AND GURSUL, I. 2020 Three-dimensional instabilities of vortices shed from a plunging wing: Experiments, *Bulletin of the American Physical Society*, the 73rd Annual Meeting of the APS Division of Fluid Dynamics (APS DFD 2020), 22-24 November 2020, virtual meeting.

SON, O., WANG, Z. AND GURSUL, I. 2021a Three-dimensional instabilities of vortices on a periodically plunging wing, AIAA 2021-1211, *AIAA Science and Technology Forum and Exposition (SciTech 2021)*. Nashville, Tennessee, USA, 11-15 January 2021.

SON, O., GAO, A., GURSUL, I., SHERWIN, S. J., WANG, Z. AND CANTWELL, C. D. 2021b Leading-edge vortices on plunging airfoils and wings, *in preparation for publication*.

SQUIRE, H. B. AND YOUNG, A. D. 1937 The calculation of the profile drag of aerofoils, *Aeronautical Research Committee Reports and Memoranda*, **1838**.

SUN, L., DENG, J. AND SHAO, X. 2018 Three-dimensional instabilities for the flow around a heaving foil, *Phys. Rev. E.*, **97** (1-1).

THEODORSEN, T. 1935 General theory of aerodynamic instability and the mechanism of flutter, *NACA Tech. Rep. 496*.

TRIANTAFYLLOU, M.S., TRIANTAFYLLOU, G.S. & GOPALKRISHNAN, R., 1991, Wake mechanics for thrust generation in oscillating foils, *Physics of Fluids A: Fluid Dynamics*, **3**, 2835-2837 https://doi.org/10.1063/1.858173

TURHAN, B., WANG, Z. AND GURSUL, I. 2020 Structure of tip vortex and wake of unsteady wings, AIAA 2020-0349, *AIAA Science and Technology Forum and Exposition (SciTech 2020)*. Hyatt regency Orlando, Orlando, Florida, USA, 6-10 January 2020.

VISBAL, M. R. 2009 High-fidelity simulation of transitional flows past a plunging airfoil, *AIAA J.*, **47** (11), pp. 2685-2697.

VON KARMAN, T. H. AND SEARS, W. R. 1938 Airfoil theory for non-uniform motion, *Journal of the Aeronautical Sciences*, **5** (10), pp. 379–390.

WEI, T. & SMITH, C.R., 1986 Secondary vortices in the wake of circular cylinders, *Journal of Fluid Mechanics*, **169**, pp. 513-533.

WEI, N. J., KISSING, J. AND TROPEA, C. 2019a Generation of periodic gusts with a pitching and plunging airfoil, *Exp. in Fluids*, **60** (11).

WEI, N. J., KISSING, J., WESTER, T. T. B., WEGT, S., SCHIFFMANN, K., JAKIRLIC, S., HOLLING, M., PEINKE, J. AND TROPEA, C. 2019b Insights into the periodic gust response of airfoils, *J. Fluid Mechanics*, **876**, pp. 237-263.

WILDER, M. C. AND TELIONIS, D. P. 1998 Parallel blade-vortex interaction, *J. Fluids Struct*., **12**, pp. 801–838.

WILLIAMSON, C. H. K. 1996 Three-dimensional wake transition, *J. Fluid Mechanics*, **328**, pp. 345-407.

WU, Z. L., BANGGA, G., LUTZ, T., KAMPERS, G. AND HOLLING, M. 2020 Insights into airfoil response to sinusoidal gusty inflow by oscillating vanes, *Physics of Fluids*, **32** (12).

YOUNG, J. AND LAI, J. C. S. 2007 Vortex lock-in phenomenon in the wake of a plunging airfoil, *AAIA J*., **45** (2), pp. 485-490.

ZHANG, Z., WANG, Z. AND GURSUL, I. 2021 Aerodynamics of a wing in turbulent wakes, *in preparation for submission for publication*.